nature reviews earth & environment

https://doi.org/10.1038/s43017-025-00743-1

Review article

Check for updates

Insights into terrestrial carbon and water cycling from the global eddy covariance network

Jingfeng Xiao [1] ✉, Dennis Baldocchi [2], Kazuhito Ichii [3], Fei Li [4] & Dario Papale [5,6]

Abstract

Ecosystem–atmosphere exchanges of carbon dioxide (CO_2) and water vapour respond to global environmental changes, such as climate change, elevated atmospheric CO_2, disturbances, and land use change and management. Understanding these exchanges requires globally distributed and continuous, long-term ecosystem-scale measurements spanning diverse climates and ecosystems, as supported by the development of the eddy covariance (EC) technique. In this Review, we discuss how the global network of EC sites, led by FLUXNET, has advanced understanding of terrestrial carbon and water cycling. Since the early 1990s, EC measurements have provided insights into variations in carbon and water fluxes across different timescales (half-hourly to decadal), vegetation types and environmental gradients, and their responses to global change. Upscaling EC measurements and the resulting datasets have also enhanced understanding of the magnitude, spatial patterns, seasonal changes, interannual variability, and trends in carbon sinks and sources, evapotranspiration, and water-use efficiency in response to global change at regional to global scales. EC measurements and upscaled data also help interpret and evaluate satellite-derived products, as well as benchmark and improve terrestrial biosphere models and Earth system models. Future efforts should improve network representativeness, foster open data sharing, provide near real-time measurements, enhance accuracy of upscaled products and better support climate mitigation efforts.

Sections

[1]Earth Systems Research Center, Institute for the Study of Earth, Oceans, and Space, University of New Hampshire, Durham, NH, USA. [2]Department of Environmental Science, Policy and Management, University of California, Berkeley, CA, USA. [3]Center for Environmental Remote Sensing, Chiba University, Chiba, Japan. [4]Institute of Grassland Research, Chinese Academy of Agricultural Sciences, Hohhot, China. [5]Institute of Research on Terrestrial Ecosystems (IRET), National Research Council (CNR), Monterotondo Scalo, Italy. [6]Fondazione CMCC - Centro Euro-Mediterraneo sui Cambiamenti Climatici, Viterbo, Italy. ✉e-mail: j.xiao@unh.edu

Introduction

The exchanges of carbon dioxide (CO_2) and water vapour between terrestrial ecosystems and the atmosphere vary across diel (or diurnal), seasonal, annual and decadal timescales. Water and/or heat stress can cause plants to exhibit midday depression in photosynthesis and transpiration, reducing daily ecosystem carbon uptake and water loss[1–3]. Carbon and water fluxes also shift at longer timescales (seasonal, annual and decadal) in response to climate variability and change, elevated atmospheric CO_2, disturbance and management, which in turn affect the climate. Therefore, high-frequency and long-term measurements are essential for understanding ecosystem-level CO_2 and water exchanges. The eddy covariance (EC) technique can continuously measure ecosystem-level carbon and water fluxes with high frequency (half hourly or hourly)[4,5], enabling the characterization of land–atmosphere carbon and water exchanges for various plant functional types over diurnal and longer timescales.

The EC technique was first used to measure CO_2 exchange in the early 1970s[6,7], with open-path CO_2 sensors introduced in the mid-1980s[8,9] (Fig. 1). Since their development, EC measurements have demonstrated that remotely sensed vegetation indices were strongly correlated with ecosystem carbon exchange in the early 1990s[10,11] and have been used to evaluate terrestrial biosphere models in the mid-1990s[12–14] and optimize model parameters in the early 2000s[15]. Long-term EC records have also supported investigations into how climate change, rising atmospheric CO_2 and disturbances shape the long-term trends in carbon and water fluxes[16,17] in the late 2000s.

The rapid global growth of EC sites[5,18] in the mid and late 1990s led to the establishment of regional EC networks and the FLUXNET[5]—the global network of EC flux measurement sites (Supplementary Note 1). Before these networks, data were collected independently at individual sites, often processed differently and not broadly shared, which limited accessibility and comparability. The coordination of EC data across regions and the globe — through standardization, integration and open sharing of data, training of site personnel, and fostering dialogue between data providers and users — has enabled cross-site comparisons and synthesis of biosphere carbon and water fluxes across ecological and climatic gradients, disturbances and experimental manipulations[19–21]. Indeed, since its founding, FLUXNET has released three databases (Marconi 2000, La Thuile 2007 and FLUXNET2015 (2015))[20] (Fig. 1), with increasing quality, data variety and number of site-years. For example, a global synthesis revealed that old-growth forests, even up to 400 years old, can continue to sequester carbon, challenging the long-standing view that they are carbon neutral[22]. EC data have also been upscaled to regional and global fluxes using machine learning approaches[23–26], enabling broad-scale assessments of carbon and water cycles, interpretation and evaluation of satellite-derived products, and benchmarking and improvement of terrestrial biosphere models and Earth system models.

Since the late 2010s, the availability of additional EC flux measurements, more advanced diagnostic, attribution and upscaling methods, powerful computational platforms such as cloud computing, and emerging satellite observations have facilitated research and applications driven by EC flux data. However, no study has thoroughly reviewed how EC data have advanced terrestrial carbon and water cycle research from the ecosystem to the global scale. Ecosystem-level carbon and water cycling[27,28] or upscaling methods[29,30] have been reviewed; however, despite these contributions (Supplementary Fig. 1), there has been no overview or synthesis of the role of EC data in progressing understanding of carbon and water cycling at regional to global scales.

In this Review, we examine how EC measurements and the global flux network have contributed to terrestrial carbon and water cycle research. We discuss how EC measurements and upscaled data have advanced understanding of carbon and water cycling. We also review flux upscaling methods, EC data limitations and uncertainties; how these data support the evaluation of satellite-derived products and model development; and recommend ways to enhance networks, improve data sharing and refine upscaled products to better support future applications.

Diel to annual carbon and water cycling

Carbon and water flux measurements derived from the EC technique (Box 1) have greatly advanced understanding of ecosystem-level carbon and water cycling[27,31] by supporting the formulation and testing of hypotheses, addressing fundamental science questions, enabling synthesis and facilitating exploratory analyses. This section discusses what EC measurements have revealed about diel and seasonal variations and annual fluxes.

Diel variations

The EC technique is capable of continuously measuring ecosystem-level carbon and water fluxes at half hourly (or hourly) intervals for various plant functional types, enabling characterization of land–atmosphere exchanges over diel to longer timescales. For instance, EC measurements have uniquely revealed how carbon and water fluxes at the ecosystem scale vary over the course of the diel cycle in response to environmental conditions[32,33] (Fig. 2a). Gross primary production (GPP) and evapotranspiration (ET) generally exhibit diel patterns that closely follow the course of photosynthetically active radiation (PAR), with peak fluxes occurring near midday[34]. These patterns are also influenced by air temperature, soil moisture and vapour pressure deficit (VPD), and regulated by stomatal conductance[35]. Both GPP and net carbon uptake increase with PAR, eventually reaching a plateau at the light saturation point[32]. Moreover, plants often show larger responses to PAR in the morning than in the afternoon at a given light intensity[32]. Therefore, GPP and ET can exhibit hysteresis in their responses to environmental variables, especially light[36,37].

Fig. 1 | Evolution of the global network of EC flux sites. a, Milestones for the global flux network, FLUXNET. **b**, The distribution of the eddy covariance (EC) sites included in the Marconi database (2000). The base map is the Moderate Resolution Imaging Spectroradiometer (MODIS) land cover map, and the vegetation types are as follows: evergreen needleleaf forests (ENF), evergreen broadleaf forest (EBF), deciduous needleleaf forest (DNF), deciduous broadleaf forest (DBF), mixed forest (MF), closed shrubland (CSH), open shrubland (OSH), woody savannas (WSA), savannas (SAV), grassland (GRA), wetland (WET) and cropland (CRO). **c**, The distribution of EC sites included in the FLUXNET2015 database (2015). The base map shows annual precipitation over 1991–2020. **d**, The distribution of the EC sites included in the regional networks as of January 2025. The base map shows annual mean temperature (°C) over 1991–2020. **e**, The percentage of sites for each vegetation type for each database and the percentage of land area for each vegetation type. References for the milestones and data sources are provided in Supplementary Table 1. The global EC flux network has evolved since the 1990s and its spatial coverage and ecosystem representativeness have greatly improved since 2000. ET, evapotranspiration; GPP, gross primary production; ICOS, Integrated Carbon Observation System; NEON, National Ecological Observatory Network; SIF, solar-induced chlorophyll fluorescence; TERN, Terrestrial Ecosystem Research Network; USCCC, US–China Carbon Consortium.

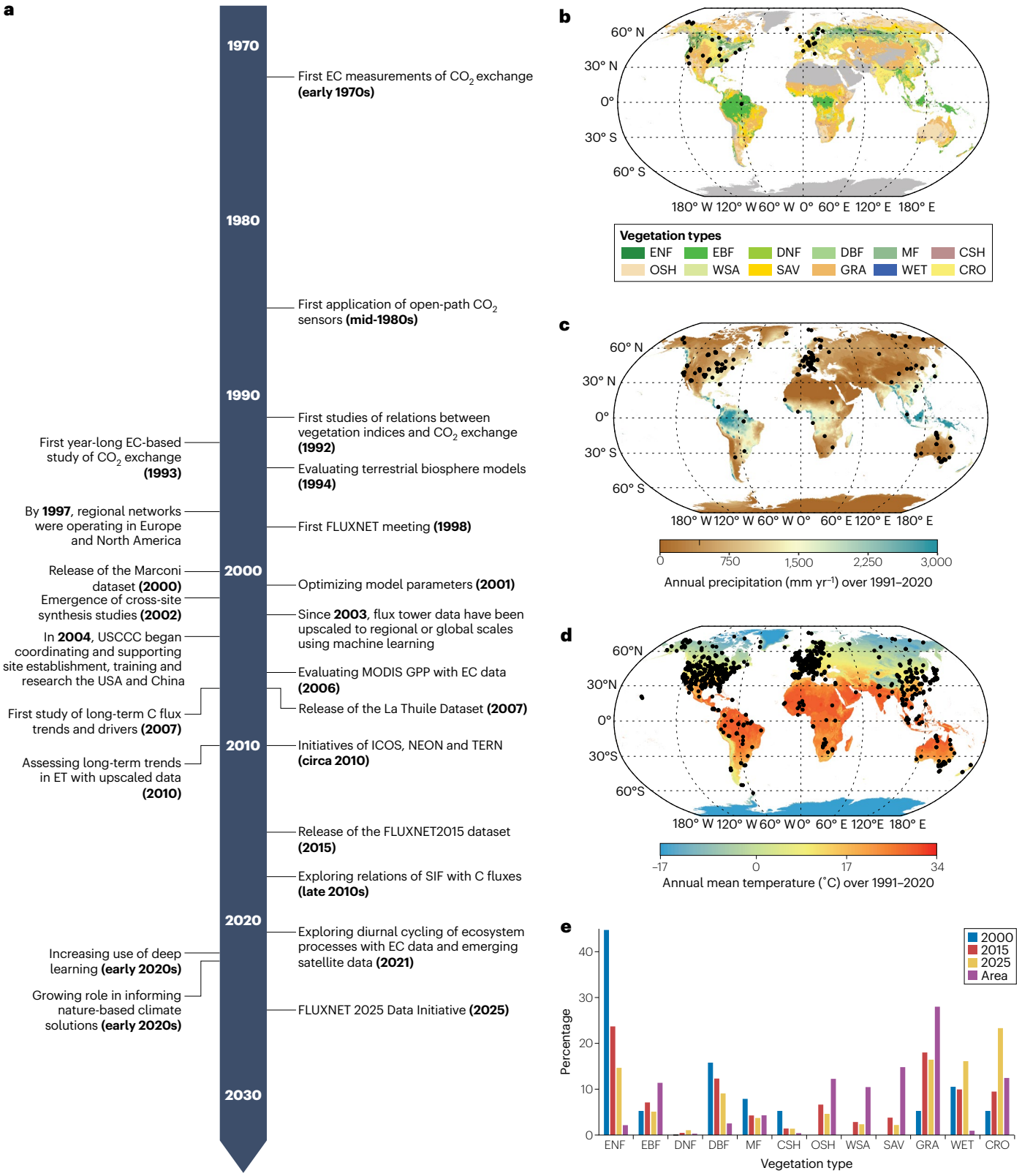
a
1970
1980
1990
2000
2010
2020
2030
First EC measurements of CO_2 exchange (early 1970s)
First application of open-path CO_2 sensors (mid-1980s)
First studies of relations between vegetation indices and CO_2 exchange (1992)
Evaluating terrestrial biosphere models (1994)
First FLUXNET meeting (1998)
Optimizing model parameters (2001)
Since 2003, flux tower data have been upscaled to regional or global scales using machine learning
Evaluating MODIS GPP with EC data (2006)
Release of the La Thuile Dataset (2007)
Initiatives of ICOS, NEON and TERN (circa 2010)
Release of the FLUXNET2015 dataset (2015)
Exploring relations of SIF with C fluxes (late 2010s)
Exploring diurnal cycling of ecosystem processes with EC data and emerging satellite data (2021)
FLUXNET 2025 Data Initiative (2025)
First year-long EC-based study of CO_2 exchange (1993)
By 1997, regional networks were operating in Europe and North America
Release of the Marconi dataset (2000)
Emergence of cross-site synthesis studies (2002)
In 2004, USCCC began coordinating and supporting site establishment, training and research the USA and China
First study of long-term C flux trends and drivers (2007)
Assessing long-term trends in ET with upscaled data (2010)
Increasing use of deep learning (early 2020s)
Growing role in informing nature-based climate solutions (early 2020s)
b
60° N
30° N
0°
30° S
60° S
180° W 120° W 60° W 0° 60° E 120° E 180° E
Vegetation types
ENF EBF DNF DBF MF CSH
OSH WSA SAV GRA WET CRO
c
60° N
30° N
0°
30° S
60° S
180° W 120° W 60° W 0° 60° E 120° E 180° E
0 750 1,500 2,250 3,000
Annual precipitation (mm yr⁻¹) over 1991–2020
d
60°N
30°N
0°
30°S
60°S
180° W 120° W 60° W 0° 60° E 120°E 180° E
−17 0 17 34
Annual mean temperature (°C) over 1991–2020
e
Percentage
0 10 20 30 40
2000
2015
2025
Area
ENF EBF DNF DBF MF CSH OSH WSA SAV GRA WET CRO
Vegetation type

Box 1 | EC and FLUXNET data

The eddy covariance (EC) method is a micrometeorological technique that directly measures CO_2, water vapour and energy flux densities (in mol m^{-2} s^{-1}) between the atmosphere and the underlying vegetation and soil[18,251,254]. Measurements are made using EC flux towers across a range of ecosystem types, including forests[255] (left figure panel, courtesy of André Künzelmann), shrublands, savannas, croplands (central figure panel, courtesy of Gang Dong), grasslands, and wetlands[256] (right figure panel, courtesy of the FI-Sii team). Applied to an individual ecosystem, the EC method measures the breathing of the ecosystem on timescales from half hourly, to days, seasons, years and decades. The ground area that the EC measurements represent, called the flux footprint, typically spans from a hundred metres to several kilometres[257,258].

EC measurements include net ecosystem exchange of CO_2, latent heat flux and sensible heat flux, which are typically quality controlled and gap filled using standardized processing procedures[20]. Net ecosystem exchange measurements are routinely partitioned into gross primary production and ecosystem respiration using night-time and/or daytime partitioning approaches. The latent heat flux is converted to evapotranspiration by dividing it by the latent heat of vaporization. Each EC site is usually equipped with other instruments that measure meteorological variables, such as temperature, precipitation, solar radiation and relative humidity, as well as soil temperature and soil moisture. The EC technique has also been used to measure the exchange of other greenhouse gases including methane (CH_4) and nitrous oxide (N_2O)[259].

There are over 1,000 sites worldwide where EC measurements of carbon and water fluxes are available[260]. These sites are coordinated by regional networks (such as AmeriFlux, EuroFlux and AsiaFlux), international consortiums (for example, the US–China Carbon Consortium), and a global network (FLUXNET; Supplementary Note 1). The availability of EC measurements has also led to the generation of gridded flux data products through upscaling to regional and global flux products, such as EC-MOD[121], FLUXCOM[119] and MF-CW[26], which are higher-level FLUXNET datasets.

High-frequency measurements from EC sites have demonstrated that plants can shut down stomata under conditions of low soil moisture, high temperature or elevated VPD, particularly around midday[38,39]. This response leads to midday depressions in ET and GPP, and shifts in their diurnal centroids towards the morning[40]. This phenomenon becomes more pronounced in dry climates and during droughts or heatwaves, resulting in substantial declines in daily ET and GPP[35,38,41]. For example, heatwaves induced daily average GPP anomalies (*z*-scores) ranging from −0.30 to −0.45 in forests, and from −1.16 to −0.84 in shrublands across the Northern Hemisphere[35]. The extent to which ecosystems have midday depressions depend on environmental conditions, groundwater availability, vegetation type and species-specific physiological responses[35].

Seasonal variations

EC measurements enable the determination of the onset, end and length of the growing season[42]. Although these timings can also be derived from satellite-derived vegetation indices and field-based phenology observations, continuous EC measurements also capture seasonal variations in carbon uptake, respiration and ET at the ecosystem scale that cannot be directly observed by other methods. Ecosystems generally act as carbon sinks during the growing season and as carbon sources or remain carbon neutral during the rest of the year. Most ET also occurs during the growing season due to transpiration. For example, in a Mediterranean grassland, diel net ecosystem exchange (NEE) patterns show strong carbon uptake from February to April, with midday uptake declining as rainfall ceases and soils dry (Fig. 2a). Ecosystem assimilation is complemented by ecosystem respiration (RECO)[43], which peaks at night during periods of high daytime carbon uptake (Fig. 2a), showing that RECO and GPP co-vary (or are coupled)[44].

Temperature strongly influences soil respiration when soils are moist[45,46]. In drylands, episodic respiration pulses triggered by rain events were often missed before continuous EC measurements[47–49].

Photodegradation can also contribute to post-rain respiration bursts[50]. Soil water availability and/or VPD influence carbon and water fluxes[51–53]. For example, low soil moisture decreases GPP across climate zones[51,53], whereas high VPD during rain pulses can suppress GPP more than RECO or ET in drylands[52]. The influence of soil moisture deficits on NEE can be assessed through its relationship with evaporative fraction (Fig. 2b). Root systems convey information on soil moisture status and groundwater access, regulating the capacity of plants for transpiration and photosynthesis[54,55].

Droughts and heatwaves typically reduce ET, GPP and net carbon uptake due to low soil moisture and/or high VPD — and even trigger net carbon releases — altering their seasonal patterns[56–58]. Continuous flux, meteorological and soil moisture measurements from EC sites have captured these responses by directly recording shifts in ET, GPP and net carbon uptake, as well as changes in soil moisture and VPD to reveal how extreme events modify seasonal flux dynamics. In energy-limited ecosystems, however, increases in air temperature and light availability during drought could increase carbon uptake[59]. Flash droughts lower GPP[60] and often begin with increased ET driven by elevated VPD, followed by rapid declines in soil moisture and ET[61]. Disturbances such as wildfire and insect outbreaks also disrupt seasonal fluxes[62]. For example, insect outbreaks can reduce GPP more than RECO, thereby lowering net carbon uptake for months[63], and can also reduce ET by decreasing the leaf area index (LAI)[64]. Unlike other approaches, such as remote sensing, continuous EC measurements capture these ecosystem-level responses in carbon and water cycling.

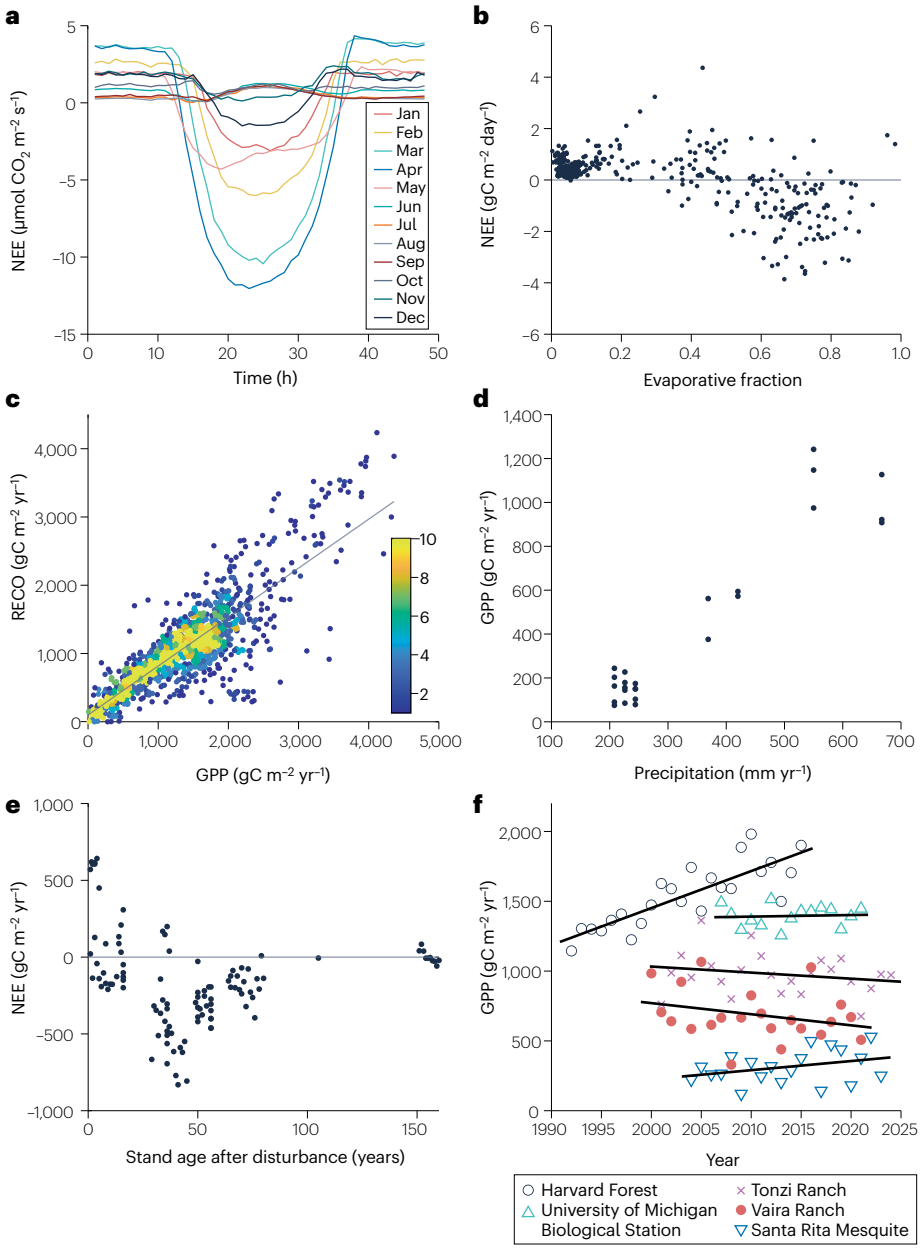

Fig. 2 | Variations in ecosystem-level carbon fluxes across time and space. a, Diel variations of net ecosystem exchange (NEE) for each month at Vaira Ranch, a grassland site in California, USA. Negative NEE represents a loss of carbon from the atmosphere but a gain by the ecosystem. **b**, Changes in daily NEE with the evaporative fraction at Vaira Ranch. High water stress (lower evaporative fraction) led to reduced net carbon uptake or net carbon release. **c**, Annual sums of ecosystem respiration (RECO) are tightly coupled with those of gross primary production (GPP). **d**, The relationship between annual GPP and annual precipitation based on eddy covariance measurements from a group of sites along an elevation gradient in New Mexico, USA. **e**, Changes of annual NEE with stand age following stand-replacing disturbances based on conifer sites in Canada and the Pacific Northwest. **f**, Long-term changes in annual GPP across five sites in a changing environment. Data sources are provided in Supplementary Table 2. Continuous, high-frequency eddy covariance data from numerous sites reveal ecosystem responses to environmental factors, disturbance and elevation at various temporal scales (half-hourly, daily, seasonal, annual and decadal) and spatial scales.

Annual fluxes

When the first annual EC measurements started in the early 1990s, it was poorly understood how much carbon an ecosystem could assimilate or how much water it could transpire annually[4,65–67]. Since then, several thousand site-years of annual sums have been published and are available for distillation. Annual NEE has a median of −181.5 gC m^{-2} yr^{-1}, with the most productive ecosystems sequestering as much as 1,000 gC m^{-2} yr^{-1} or more, but with disturbed ecosystems losing up to 700 gC m^{-2} yr^{-1} (Supplementary Fig. 2). Annual ET ranges from ~50 to 1,400 mm yr^{-1}, with a median of 438.8 mm yr^{-1} (Supplementary Fig. 3). A key constraint is that annual ET typically does not exceed annual precipitation (Supplementary Fig. 4). When moisture is ample, ET becomes energy limited, as reflected by potential ET[68,69]. However, in arid and semi-arid regions, ET can exceed precipitation in riparian zones and areas supported by groundwater or irrigation as plants access water sources beyond precipitation[70]. EC data facilitate the direct measurement of such changes in ET and how tightly it tracks available energy in humid ecosystems and diverges in groundwater-fed or irrigated systems.

Coordinated through regional networks and FLUXNET, EC measurements from geographically diverse regions and various plant functional types have enabled large-scale comparisons, revealing many biophysical factors causing the range in annual fluxes. Plant functional type is one key factor associated with distinct climate spaces[28,71,72]. These climate spaces have distinct patterns and ranges in temperature, rainfall and absorbed sunlight, which affect growing season length and rates of photosynthesis, respiration and transpiration[73]. Photosynthesis and respiration are tightly coupled, and factors increasing photosynthesis also increase respiration, and vice versa[28,31]. Ecosystems with the longest growing season and higher LAI are among the most productive and transpire the most[74] (for example, annual terrestrial carbon uptake and ET increased with growing season length in China[75]). However, increases in carbon uptake and ET from earlier springs could be offset by summer droughts. For example, in the conterminous USA, decreased carbon uptake during the 2012 summer drought offset the earlier spring carbon gains induced by warming, and soil moisture depletion from increased spring ET enhanced summer heating through land–atmosphere coupling[76].

A key lesson learned by comparing carbon flux data is how tightly annual GPP and RECO are coupled (Fig. 2c). On average, nearly 80% of carbon fixed through photosynthesis is returned to the atmosphere as respiration[28,31]. This finding indicates that biological and/or engineering efforts to enhance photosynthesis will come at the cost of more respiration, leading to lower-than-expected net carbon uptake. Therefore, without addressing this balance, such efforts might not achieve the desired carbon sequestration, potentially limiting their effectiveness in mitigating climate change. Another important finding from EC data is that assimilation and transpiration are tightly coupled, as first demonstrated across FLUXNET sites in 2002[77] and reaffirmed by global cross-site syntheses using expanded datasets[78]. This tight coupling between GPP and ET demonstrates that both fluxes are jointly regulated by stomatal conductance[79] and reveals that ecosystems assimilate more carbon at the cost of greater water consumption.

Measurements based on regional networks showed that ecosystem carbon uptake and ET vary substantially along ecological, climate, and elevational gradients[70,80] that influence temperature and precipitation patterns[81]. For example, the measurements along an elevational gradient in a semi-arid region indicated that a 400 mm range in annual precipitation can result in a 1000 gC m^{-2} yr^{-1} range in GPP (Fig. 2d). Along an elevation gradient of nearly 3,000 m spanning oases and deserts to alpine ecosystems, annual ET ranges from 200 to 1,200 mm yr^{-1} (ref. 70).

Interannual flux variability and trends

Long-term flux measurements provide critical insights into how ecosystem carbon and water exchanges respond to global change. These fluxes often show substantial interannual variability and long-term trends under the influence of one or more global change factors. These trends and variability are discussed in this section.

Interannual variability

Climate variability and change, particularly extreme climate events, can lead to substantial interannual variability in carbon and water fluxes, as revealed by multi-year measurements from EC sites. Interannual temperature variability can alter annual carbon fluxes by modulating photosynthetic and respiratory activity[82], as well as phenological timing and growing season length[83]. For example, early leaf emergence resulting from warm springs can enhance annual GPP and net carbon uptake[83], and warmer years can also increase atmospheric demand for water via higher VPD and net radiation, and enhance annual ET[84]. Heatwaves can reduce annual GPP and ET by decreasing stomatal conductance and/or causing leaf mortality and lower LAI[85]. Cold springs delay leaf unfolding, leading to shorter growing seasons and, together with low annual precipitation, resulted in substantially reduced annual GPP, ET and net carbon uptake at a managed, even-aged mature forest site in Germany[86].

Multi-year EC measurements have further demonstrated that precipitation variability can also cause substantial variability in carbon and water fluxes. In wetter years, higher precipitation and soil moisture often increase ET and stimulate GPP more than RECO, enhancing net carbon uptake[87,88]. Under cloudy conditions, photosynthesis is more sensitive to diffuse light[89]. The seasonal distribution of precipitation can be more important than annual precipitation, as a large fraction of precipitation occurring in the summer reduces moisture stress and promotes transpiration and photosynthesis[90]. In the Amazon, for instance, photosynthesis responded weakly to seasonal precipitation, whereas respiration responded strongly, with the highest value in the wet season and the lowest in the dry season[91]. Drought can reduce stomatal conductance, induce early leaf senescence, and thereby suppress transpiration and photosynthesis, leading to lower annual ET and GPP[84]. Heatwave and drought compound events could result in reduced GPP along with lower ET and soil drying, leading to reduced carbon uptake or even a net carbon source. For example, during the 2003 European heatwave and drought, EC measurements from multiple sites showed large reductions in GPP and small decreases in RECO, temporarily turning Europe from a carbon sink to a carbon source[92].

Disturbances such as insect outbreaks, hurricanes, wildfire and logging[63,93] can reduce GPP and/or increase RECO, lowering net carbon uptake or even resulting in net carbon losses, as revealed by multi-year EC measurements. Insect outbreaks can defoliate forest canopies, reducing annual GPP and net carbon uptake[94] as well as ET[64]. Hurricanes cause defoliation and tree mortality, and lead to much lower GPP, increased RECO and reduced net carbon uptake[95]. Following a stand-replacing windthrow, the cumulative ET during the snow-free season in a larch forest decreased by 24% during the following year and returned to pre-disturbance levels within 5 years[96].

Very few EC sites, if any, have experienced stand-replacing disturbances with measurements both before and after the events, and

no site has yet covered the complete life cycle of a forest ecosystem. However, the chronosequence approach, enabled by availability of flux measurements for a number of sites with similar climatic and soil conditions but with different stand age following wildfire, logging, or other stand-replacing disturbances, shows that ecosystem carbon uptake increases with stand age up to a point and then declines[22,93,97] (Fig. 2e). These studies provide a test of foundational ecological theory[98,99], suggesting that stand age must be considered in ecosystem carbon-balance modelling. They also showed that ageing forests might still serve as a carbon sink[22] but might not be able to take up as much carbon as in the past[100]. Nevertheless, from the life cycle carbon-balance perspective, old-growth forests have already accumulated substantial carbon stocks in plants and soils over time.

Long-term trends

A select group of flux datasets are starting to exceed two or three decades in length, revealing various temporal patterns of null, positive and negative responses with time (Fig. 2f). Analyses based on measurements from globally distributed EC flux sites indicate that elevated CO_2 enhanced photosynthesis and net carbon uptake via the CO_2 fertilization effect and indirectly through increases in LAI[101,102]. Meanwhile, elevated CO_2 can reduce stomatal conductance and lower transpiration[102], contributing to greater soil moisture retention and water yield. The resulting enhancement of GPP and suppression of ET can increase water-use efficiency (WUE), as demonstrated by EC measurements across 21 temperate and boreal forest sites[103]. However, the effects of elevated CO_2 on ecosystem carbon fluxes are not fully understood, and some evidence indicates that the CO_2 fertilization effect might have declined, or that elevated CO_2 does not always lead to a clear increase in photosynthesis. For example, GPP estimates from 22 EC flux sites suggest an average decline in the CO_2 fertilization effect of −0.70% per 100 ppm CO_2 yr^{-1}, confirming results based on satellite-derived vegetation indices and LAI[104]. A global synthesis of EC measurements from 78 sites showed no widespread trend in canopy conductance under elevated CO_2[105]. However, because the enhancement could be constrained or offset by nitrogen limitation[106], further research is needed to clarify the effects of elevated CO_2.

Multi-year to multi-decadal EC flux measurements have also provided valuable insights into long-term trends in response to climate change. Warmer temperatures can lead to increasing trends in ecosystem carbon uptake by enhancing photosynthesis rates and/or extending the growing season[17]. During the warming hiatus (1998–2012), there were no widespread trends in spring and autumn phenology and carbon uptake across the 56 Northern Hemisphere sites with at least 7 years of high-quality EC data[107]. Warmer temperatures also lead to higher VPD, which can reduce GPP[108] and can either enhance ET by increasing atmospheric demand or suppress ET by triggering stomatal closure[109]. A global synthesis of EC data revealed that increasing VPD suppressed light-use efficiency (LUE) and carbon uptake, consistent with findings from satellite-based analyses of vegetation indices, LAI and GPP[110]. Seasonal warming led to an increase in net carbon uptake for old forests (>90 years old) and a decrease in young (<40 years old) and mid-aged (40–90 years old) forests[111].

Changes in precipitation and soil water availability also shape the trends in carbon and water fluxes. For example, at a desert shrubland EC site, pre-growing season precipitation showed a strong negative correlation with both annual and growing season NEE, indicating that higher pre-growing season precipitation enhanced net carbon uptake during both periods[112]. Long-term trends in carbon and water fluxes are often driven by one or more global change factors and their complex interactions[27]. EC measurements spanning 19 years at a Mediterranean oak savanna site showed no significant trend in ET owing to many competing positive and negative feedbacks among stomatal sensitivity to CO_2 concentrations, soil moisture and VPD, as well as temperature effects on saturation vapour pressure and plant access to groundwater[54]. No significant trends in ET were observed at 46 of 67 FLUXNET sites from 1995 to 2014, reflecting complex interactions among climate, vegetation and soil water availability[113].

Upscaling EC measurements

Although EC measurements are invaluable for research on carbon and water cycles, they capture flux exchanges only within the footprint, a relatively small area around the tower[114]. These measurements have been widely upscaled to regional and global fluxes.

Rationale and procedures

The findings achieved at individual EC sites do not necessarily apply elsewhere. Moreover, altogether, the EC sites sample only a tiny portion of the global land surface (Fig. 1d). Generating flux estimates for areas not sampled by EC sites can enable investigation of ecosystem carbon and water exchanges in these areas. Moreover, regional- to global-scale studies often require flux estimates that are continuous, both spatially and temporally[115]. EC tower data therefore have been upscaled to regional[23,24,116,117] and global[25,26,118,119] flux estimates (GPP, RECO, NEE and ET) with varying spatial resolutions from 500 m (or finer) to 0.5° and time intervals from subdaily to monthly.

The upscaling of EC measurements typically relies on satellite-derived ecological data, meteorological reanalysis data and upscaling methods, and involves the following steps[24] (Fig. 3): first, a site-specific dataset comprising the target variable (carbon or water flux) and its explanatory variables for multiple EC sites is compiled and divided into a training subset and a test subset. Second, an upscaling model, typically a machine learning model (or an ensemble of models), for predicting the target variable is trained with the training subset. Third, the test subset is used to evaluate the model performance with statistical metrics such as root mean squared error and coefficient of determination (R^2). When the compiled dataset is relatively small, cross-validation is often used. Finally, the predictive model with a satisfactory performance is used to generate spatially and temporally continuous flux estimates. Satisfactory performance has no fixed threshold as it depends on multiple factors such as the flux variable, site representativeness and region; for example, R^2 thresholds are generally lower for NEE than for GPP or ET as NEE is typically more challenging to estimate.

Requirements for EC measurements

To develop predictive carbon and/or water flux models that are applicable for a study domain, it is important to have measurements from a number of sites — typically as many as possible — that are representative of the study domain in terms of ecosystem and climate types and disturbance history. For example, a total of 25, 94 and 187 sites were used to upscale tower measurements for the Tibetan Plateau[120], North America[121] and the globe[26], respectively. It is recommended to use good-quality flux measurements from all the sites within the region. Should insufficient data be available, measurements from other regions with similar characteristics can also be used. Besides spatial representativeness[122,123], temporal representativeness[124] is also essential for developing reliable predictive models. The availability of long-term

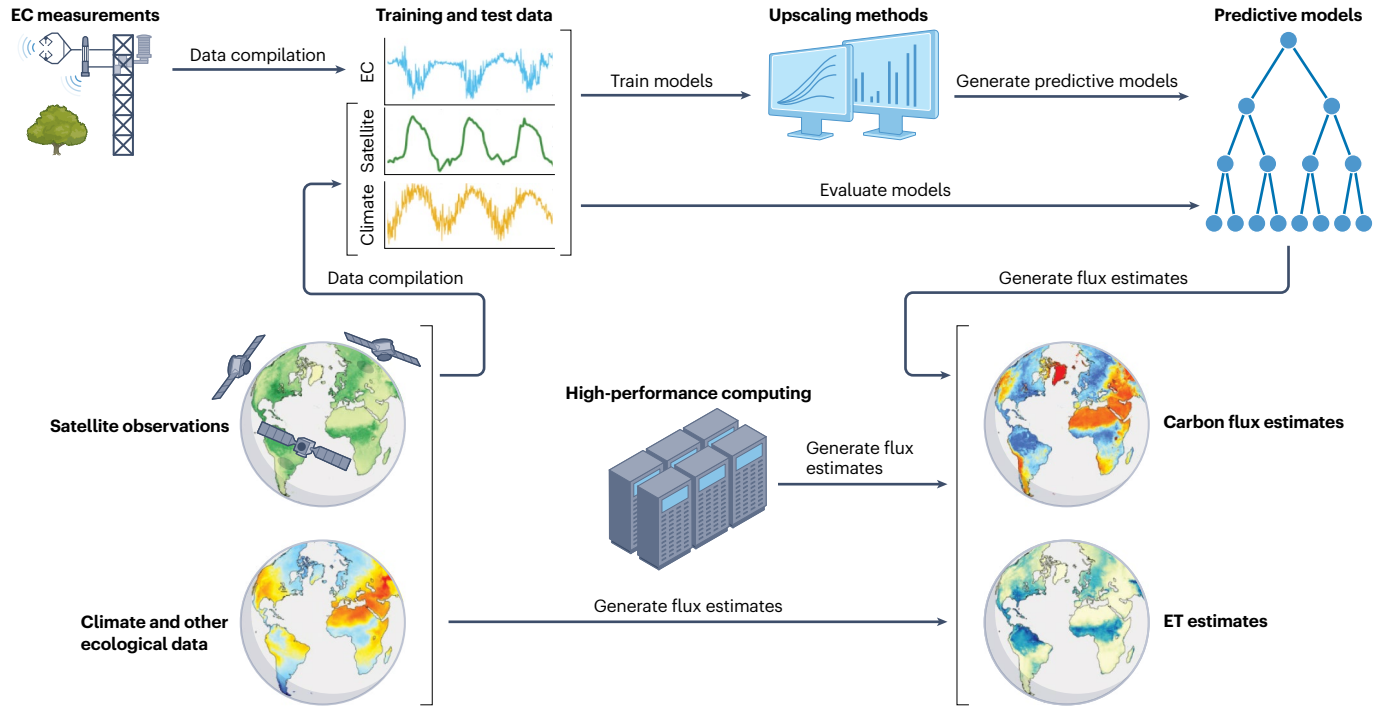

Fig. 3 | Procedures for upscaling EC flux measurements. This multi-step process enables the spatial and temporal scaling of site-level eddy covariance (EC) flux data to regional or global scales, supporting large-scale assessments of terrestrial carbon and water cycling. ET, evapotranspiration.

flux measurements generally can improve the model's performance in capturing interannual variability and long-term trends.

Explanatory variables

The selection of explanatory variables for machine learning models should be guided by ecological principles, and environmental and ecological factors that control the target variable (GPP, RECO, NEE or ET) are typically chosen. For example, photosynthesis models such as Farquhar model[125] and LUE logic[126] are commonly used to guide variable selection for upscaling GPP. Vegetation type; vegetation indices such as the enhanced vegetation index, **LAI**, fraction of photosynthetically active radiation absorbed by canopies and land surface temperature; and meteorological variables are often chosen for upscaling GPP[127,128]. Some studies also use stand age[121,129] and aboveground biomass[121] to better account for forest status, and canopy nitrogen[121] and nitrogen deposition[129] for nutrient availability. Canopy structural complexity metrics derived from space-borne LiDAR also helps improve upscaling of GPP and ET data[130].

Each variable should have spatially and/or temporally continuous data for the study domain to ensure that fluxes can be estimated for each location and each time step. Including more predictor variables in an machine learning model will probably improve statistical measures (R^2 and root mean squared error)[130], but incorporating too many variables is not the best practice; the reason being that regional or global datasets often have substantial uncertainty, and incorporating an additional predictor can introduce another source of uncertainty to the resulting flux estimates. Some variables such as biomass, soil organic carbon and stand age can contain substantial uncertainty, and their incorporation is likely to introduce a large source of uncertainty[121].

Tower footprint and fetch area

The EC tower footprint (the upwind source area contributing to measured fluxes[131]) typically ranges from tens of metres to several kilometres[132], depending on turbulence strength, surface roughness, measurement height and atmospheric stability[133]. Ideally, the footprint should align spatially and temporally with the corresponding satellite pixel for effective upscaling. In practice, this alignment is often difficult to achieve[134]. Moreover, towers should be placed on flat, homogeneous terrain, with fetches exceeding the footprint to ensure data quality[131], but many sites are heterogeneous[131] (footprint dynamics and their influences on flux upscaling are described in detail in Supplementary Note 2). Regional to global upscaling typically uses moderate-resolution satellite data (1 km or coarser) and EC footprints are usually smaller than a single pixel; therefore satellite data from the tower pixel are matched to EC fluxes[24–26]. When high-resolution satellite data (several to tens of metres) are available, pixels within the tower footprint can be aggregated — often by weighted averaging — to better match fluxes[135]. However, because the footprint varies with wind direction and other factors (Supplementary Fig. 5), dynamically matching it to high-resolution data remains challenging.

Upscaling methods and predictions

The upscaling of EC measurements is typically based on machine learning methods, such as rule-based ensemble regression models (for example, Cubist)[24,118,121,127], artificial neural networks[23,136], model tree ensemble[25,128,129], random forest[137,138], support vector machine[139–141], extreme gradient boosting[120,142] and deep learning[116,142–144]. Interpretable machine learning methods such as rule-based models and decision trees make it easier to understand how models arrive at their

predictions. Some methods, such as artificial neural networks, are less interpretable as they operate as black boxes but have a large degree of flexibility. Some studies used multiple machine learning methods to obtain ensemble estimates[26,119,145]. Comparisons of multiple machine learning methods indicate that machine learning approaches typically have similar performances[26,120]. Although deep learning did not perform better than traditional methods in some comparison studies[116,142], the Long Short-Term Memory (a deep learning model) demonstrated a higher performance than random forest in upscaling NEE by better capturing memory effects of environmental factors[146].

Besides machine learning, LUE and process-based models have also been applied to estimate carbon and water fluxes at broad scales by calibrating uncertain model parameters with EC measurements[147–149]. Generating gridded flux estimates with these optimized models provides an alternative upscaling approach. However, the resulting estimates are often treated as model simulations rather than upscaled data[150] (Supplementary Note 3).

Computation on a desktop computer might be feasible if the spatial domain is relatively small and/or coarse spatial and temporal resolutions are used, but the estimation of carbon or water flux over broad regions with the trained and evaluated model is typically conducted on high-performance computing facilities such as Linux clusters and supercomputers. Cloud-computing platforms have great potential for upscaling as they possess massive computing and storage capacity, and also host many satellite and meteorological data required by upscaling. The upscaled carbon and/or water flux estimates can then be used to assess ecosystem carbon and water dynamics at regional to global scales, evaluating and interpreting satellite-derived products, and benchmarking and improving terrestrial biosphere models.

Regional to global carbon cycling

Upscaling EC measurements offers an independent and alternative approach to assessing carbon cycling across regional to global scales, complementing inventory methods, terrestrial biosphere models and atmospheric inversions[115]. Upscaled flux estimates have been widely used to assess the magnitude, spatial patterns, seasonal variations, interannual variability and trends of carbon fluxes, and to understand their responses to climate change, elevated CO_2, disturbances and management practices on broad scales.

Carbon uptake capacity

Upscaled data have been used to examine the spatiotemporal patterns in GPP, RECO and NEE over regional[121,127,140,151] and global[26,128] scales, identifying when and where ecosystems are photosynthetically active versus dormant and whether they act as net carbon sinks or sources. Moreover, upscaled data show how carbon fluxes respond to factors such as temperature, precipitation, soil moisture, phenology, and vegetation type seasonally and spatially[152,153]. For example, croplands, grasslands, savannas and shrublands experience greater reductions in GPP during droughts and heatwaves, whereas forests tend to be less sensitive[154]. Spring droughts suppress peak GPP in arid regions but can enhance it in humid regions, whereas summer droughts consistently reduce peak GPP[152]. Annual GPP varies widely across regions and continents (Supplementary Fig. 6). It is highest in tropical forests (2,300 gC m^{-2} yr^{-1}); moderate in tropical savannas and grasslands, temperate forests, croplands and wetlands (1,000–1,100 gC m^{-2} yr^{-1}); lower in boreal forests and temperate grasslands and shrublands (500–600 gC m^{-2} yr^{-1}) and lowest in tundra and desert (200–300 gC m^{-2} yr^{-1})[155].

Global annual GPP was estimated to be between 106 PgC yr^{-1} (1982–2017) and over 144 PgC yr^{-1} (2000–2014)[128,153,155–157]. Tropical forests and savannas contributed 60% of this total owing to their high productivity and large land area, respectively[155]. Upscaled NEE data have also been used to quantify carbon sinks[153,158]. Strong carbon sinks were reported for the conterminous USA (−0.63 PgC yr^{-1}, 2001–2006)[158], East Asian monsoon subtropical forests (0.72 PgC yr^{-1})[159] and Australia (−0.44 PgC yr^{-1}, 2003–2022)[160], whereas a smaller sink was estimated for northern boreal forests (−0.20 PgC yr^{-1}, 2000–2018)[161]. The sink increased from boreal and Arctic regions to temperate and tropical regions, with temperature becoming more favourable, precipitation more abundant and ecosystems more productive[140]. Boreal areas were the largest carbon sink in the pan-Arctic-boreal region, whereas tundra was nearly carbon neutral[162].

Interannual variability in carbon fluxes

Carbon fluxes often have pronounced interannual variability, as revealed by upscaled data (Fig. 4a). Extreme climate events and disturbances are often attributed to be the primary sources of this variability[163,164]. For example, droughts and disturbances (such as wildfires, insect outbreaks and hurricanes) are the key drivers of interannual variability in carbon fluxes over North America, with larger variability observed in GPP than in RECO[121,158]. Notably, net carbon uptake in North America was 38.9% higher in 2005, a wet year, than in 2009, a dry year[121]. Globally, the hot spots of interannual variability in NEE were observed in Southeast Asia (monsoon rains, droughts and land-use change), southern North America (drought, heatwaves and disturbances), South America (droughts and land-use change) and the Siberian tundra (temperature shifts and changes in snow cover)[30]. GPP extremes associated with climate extremes and fires in 7% of the global land surface (1982–2011) accounted for 78% of global interannual GPP variation and a sizable portion of the NEE variation[164].

Carbon uptake in semi-arid and arid regions such as Southwest USA and Australia exhibited strong sensitivity to precipitation variability[160,165]. Drylands in central and western Australia, southwestern USA, southern Africa and Central Asia as well as regions above 60° N exhibited the highest coefficient of variation in annual GPP mainly due to low productivity and large sensitivity to water availability (Supplementary Fig. 6). These regions are particularly vulnerable to climate change, with increasing temperatures and shifting precipitation patterns affecting soil moisture and VPD, thereby influencing ecosystem carbon uptake. Hourly upscaled data showed that water and heat stress during heatwaves led to a midday depression in photosynthesis in southern Australia[1] and the western USA[166].

Long-term trends in carbon fluxes

Upscaled datasets often span two to four decades, enabling the examination of long-term trends in carbon fluxes from regional to global scales. Since the 1980s, many parts of the world — covering 50% of vegetated areas — showed increasing trends in annual GPP (Fig. 4b), leading to an increasing trend in global annual GPP (Fig. 4c). Climate change has an important role in shaping the flux trends. For example, annual GPP of global grasslands averaged 11 PgC yr^{-1} and increased by 0.023 PgC yr^{-1} (0.2% per year) over 1982–2011, primarily owing to increasing precipitation[167], and both gross and net carbon uptake increased for global semi-arid regions over 1982–2015[118].

Over Arctic tundra and boreal forests in Alaska during 2000–2011, ecosystems affected by fires between 2003 and 2011 exhibited substantial decreases in GPP (−20 gC m^{-2} yr^{-1}) and RECO (−6 gC m^{-2} yr^{-1}),

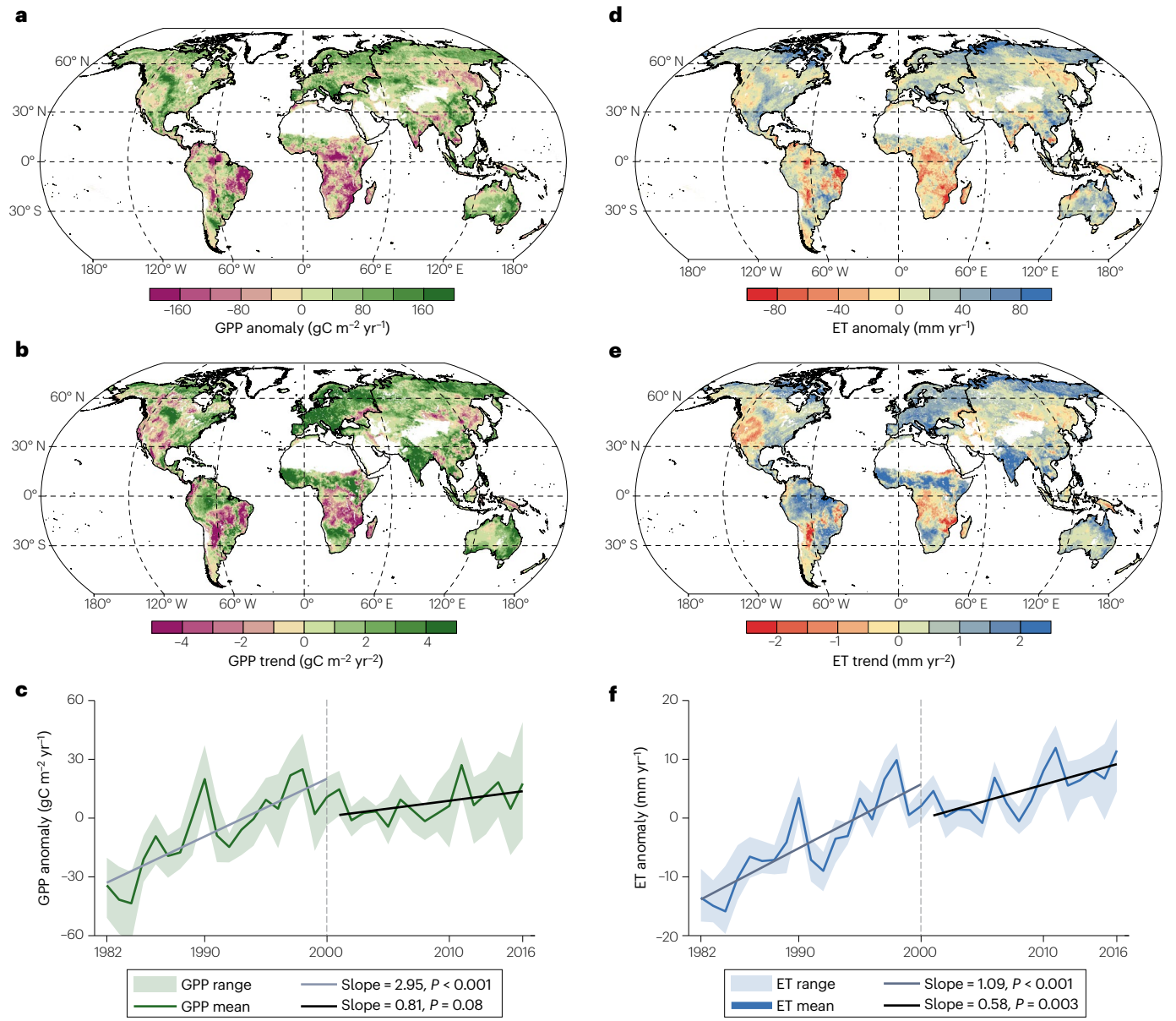

Fig. 4 | Spatiotemporal variations in annual GPP and ET across global vegetated land. a, Drought-induced gross primary production (GPP) anomalies for 2016 relative to the baseline period of 1982–2015. **b**, Spatial patterns of the trends in GPP. **c**, Fitted trends in global average annual GPP for the periods 1982–2000 and 2001–2016. **d**, Drought-induced evapotranspiration (ET) anomalies for 2016 relative to the baseline period of 1982–2015. **e**, Spatial patterns of the trends in ET. **f**, Fitted trends in global average annual ET for the periods 1982–2000 and 2001–2016. Data are based on the MF-CW product[26]. There is substantial interannual variability and significant changes in annual GPP and ET in many regions, with globally averaged values showing significant increases.

along with an increase in NEE (15 gC m^{-2} yr^{-1}), reflecting fire-induced reductions in fluxes[139]. In contrast, ecosystems burned between 1982 and 2002 (10–20 years post fire) exhibited a positive trend in GPP (20 gC m^{-2} yr^{-1}), indicating recovery that enhanced the CO_2 sink strength (−15 gC m^{-2} yr^{-1})[139]. In boreal forests, the net carbon uptake increased during 1990–2010 but slightly declined over 2011–2018 due to delayed spring snowmelt, whereas the strong increase in GPP during 1989–2018 was largely compensated by the increase in RECO[161]. The Tibetan Plateau exhibited a sustained and enhanced capacity for carbon sequestration under a warmer and wetter climate, with an increasing rate of 1.14 TgC yr^{-1} from 1982 to 2018[120]. Trends in carbon fluxes are also driven by factors such as elevated CO_2 and land management. For example, elevated CO_2 was reported to contribute to a consistent increase of global annual GPP at the rate of 0.138% ppm^{-1} from 2000 to 2014[102].

Upscaled flux data derived from EC networks also reveal decreasing or insignificant trends in terrestrial carbon uptake (Fig. 4b). Despite the overall increasing trend, the rate of increase in global annual GPP

has slowed down since 2001 (Fig. 4c), primarily due to rising VPD[26,110]. The reported decline in the CO_2 fertilization effect could have also contributed to the slowdown in the GPP increase[104]. Northern mid-latitude ecosystems experienced a 10.6% increase in negative GPP extremes during 2000–2016 compared with 1982–1998, underscoring the increasing vulnerability of ecosystem carbon uptake to warm droughts[168]. The mean temperature of the warmest quarter (3-month period) has exceeded the thermal optimum for photosynthesis, causing photosynthesis rates to decline sharply and respiration rates to continue to rise, ultimately reducing the land carbon sink[169]. The net carbon uptake of the circumpolar evergreen boreal forest did not exhibit a clear trend because the increase in GPP was offset by increasing RECO[161]. Long-term trends in carbon fluxes are jointly influenced by multiple factors, all of which have either positive or negative effects, with their combined effects varying across space and time.

Regional to global water cycling

Upscaling EC measurements offers an independent and data-constrained approach for assessing ET, a central component of the water cycle, at regional to global scales. Insights into the seasonal patterns, magnitude, interannual variability and trends of ET as well as WUE are discussed.

Seasonal and annual patterns of ET

Upscaled ET data have been used to assess the magnitude and spatial patterns of ET both regionally and globally[116,119,170]. A combination of precipitation, soil water availability, VPD, solar radiation, temperature, LAI, phenology, and management shapes the magnitude and seasonal patterns of ET, with relative importance varying across geographical regions and climate zones[171]. In water-limited regions, soil moisture is the primary constraint on ET, whereas in energy-limited regions, ET is more influenced by solar radiation and temperature[172]. ET mainly occurs during the growing season and, in regions practicing double cropping, the daily ET time series exhibits two distinct peaks within a single year[173]. ET exhibits seasonally contrasting drought responses across climate regimes. In wet regions, ET becomes decoupled from declining soil moisture and even increases during soil moisture droughts due to higher radiation and temperature, whereas in drier regions, ET decreases during droughts due to reduced soil water availability and increased plant water stress[172]. Early spring arrival often depletes soil moisture earlier in the season, causing water stress and reduced peak ET in the summer[174].

Annual ET varies substantially across vegetation types, regions and the globe (Supplementary Fig. 6). Forests and savannas exhibit the highest annual ET (701 and 697 mm yr^{-1}, respectively), croplands show intermediate ET (559 mm yr^{-1}), and grasslands and shrublands have the lowest values (388 and 304 mm yr^{-1}, respectively)[26] over the period 2001–2016 (Supplementary Fig. 6). The global annual ET estimates based on upscaled EC data are relatively consistent among studies. For example, upscaled data[119,175] estimated the mean ET for global vegetated areas over 2001–2020 at 68.9 × 10^3 km^3 yr^{-1} and 68.3 × 10^3 km^3 yr^{-1}, both of which are similar to the estimate based on the GLEAM dataset, a satellite-based ET and soil moisture product[176] (70.9 × 10^3 km^3 yr^{-1})[175]. These studies indicate that land ET returns approximately 60% of land precipitation to the atmosphere.

Interannual variability in ET

Upscaled data indicate the potential for relatively large regional and global interannual ET variability owing to climate variations, ecosystem responses and their interactions. Year-to-year changes in precipitation, solar radiation, temperature and VPD, along with soil moisture, are the main drivers of interannual ET variability[26,177]. Severe droughts can lead to widespread negative anomalies in ET. For example, the annual ET of the USA was 11.0% lower in 2002, a dry year, than in 2007, a wet year[121]. Many parts of South America and a large portion of Africa experienced relatively large negative anomalies in ET in 2016, mainly due to severe and widespread droughts (Fig. 4d). Large-scale climate oscillations such as El Niño–Southern Oscillation can modulate rainfall patterns, temperature extremes and the occurrence of storms, floods, droughts, heatwaves and wildfire, all of which can drive interannual ET variability[177,178].

Changes in vegetation phenology and LAI can also lead to interannual ET variability. For example, LAI influences interannual variability in ET globally, with particularly strong control in regions such as the eastern USA and the Amazon[179]. As the carbon and water cycles are coupled with each other, the interannual variability of ET is closely linked to that of GPP. Globally, drylands typically had a larger coefficient of variation in ET over 1982–2016 owing to their low ET and larger rainfall variability compared with humid regions (Supplementary Fig. 6).

Long-term trends in ET

Warmer temperatures increase evaporative demand and accelerate the hydrological cycle. Global annual ET increased between 1982 and 1997 due to warmer temperatures, but then declined until 2008, primarily because of increasing soil moisture limitations in the Southern Hemisphere[177]. Upscaled ET estimates in conjunction with other datasets typically showed that global ET increased since the 1980s[26,149,180–182], although the magnitude of the trends varied across the globe (Fig. 4e). The global land ET increased at a rate of 1.1 mm yr^{-1} during 1975–2017, with rising temperatures driving about 87% of this increase; humid regions, particularly the tropics, showed the highest increases (up to 7 mm yr^{-1})[181]. Anthropogenic Earth greening (afforestation) contributed to the increase in terrestrial ET[180]; elevated CO_2 reduced stomatal conductance[183], leading to lower ET. The CO_2 effect, however, could be offset by the increase resulting from warming[181] and greening[184]. Global annual ET had a stronger increase over 1982–2000 and a weaker increase over 2001–2016, and the slowdown in the ET increase was mainly due to increasing VPD[26] (Fig. 4f).

WUE

The simultaneous availability of upscaled GPP and ET estimates also enables the assessment of ecosystem WUE at regional to global scales. Forests have the highest WUE (3.0 gC kg^{-1} H_2O), followed by savannas (2.2 gC kg^{-1} H_2O), croplands (1.6 gC kg^{-1} H_2O), grasslands (1.3 gC kg^{-1} H_2O) and shrublands (1.2 gC kg^{-1} H_2O)[26]. This ranking highlights the varying efficiencies of ecosystems in converting water into photosynthetic products, with forests being the most water-use efficient in carbon uptake on an annual basis[26]. Environmental factors such as light, temperature, soil moisture, VPD and atmospheric CO_2 influence stomatal conductance, which in turn regulates photosynthesis and transpiration rates, ultimately affecting WUE[27].

WUE increases in mild and moderate drought, reflecting the physiological acclimation of plants to water stress, but decreases under severe and exceptional drought[185]. In arid ecosystems, WUE variability is mainly driven by physical processes (soil evaporation), whereas in semi-arid and subhumid regions, it is primarily influenced by biological processes (photosynthetic rate)[186]. Upscaled data also revealed significant increases in WUE in 21.8% of the global semi-arid regions[118]. There

is evidence that WUE has been increasing in response to elevated CO_2, particularly at the site level[187,188]. By contrast, a study published in 2023 using upscaled data found that global ecosystem WUE increased from 1982 to 2000 and that the increase then stalled since 2001 owing to the asymmetric effects of increasing VPD on GPP and ET[26]. A more complete understanding of carbon–water interactions requires separating total ET into evaporation and transpiration, as only transpiration is directly coupled to photosynthetic carbon uptake.

Uncertainty and wider applications

EC measurements and upscaled data have uncertainties and limitations[29,189–191], such as random and systematic errors in EC measurements and remaining inaccuracies in upscaled flux estimates. These uncertainties can introduce biases in fluxes and affect our understanding of terrestrial carbon and water cycles. Nevertheless, EC measurements and upscaled data have also greatly contributed to the interpretation and evaluation of satellite-derived products and the benchmarking and improvement of terrestrial biosphere models and Earth system models.

Uncertainty in EC measurements and upscaled data

FLUXNET and regional networks foster both a unique scientific collaboration with shared data and a large heterogeneity in data quality. As a result, measurement uncertainty has increased owing to differences in data acquisition and processing, but also to different levels of knowledge in EC requirements and set-up rules[192] (Supplementary Note 4). EC measurements have different types and sources of uncertainties. Random uncertainty, estimated at 10–20% of half-hourly measurements[189,190,193], tends to average out when fluxes are aggregated to daily to yearly sums, whereas more systematic uncertainties become increasingly important (Supplementary Note 5). Measurement uncertainty is also site dependent. For example, uncertainties in the friction velocity (u^*) threshold, NEE and RECO estimates are not directly proportional to each other or to their respective magnitudes, emphasizing the need for site-specific uncertainty assessments and thorough documentation of data processing and corrections (Fig. 5 and Supplementary Note 6). Collaborating and communicating within a large community, such as FLUXNET, can advance progress to reduce much of the uncertainty, which is often due to suboptimal site location selection, set up and processing (see Supplementary Note 7 for recommendations for reducing uncertainty).

Upscaled fluxes also have uncertainties and limitations[29] (see Supplementary Note 8 for details). Sources of uncertainty include those from EC measurements[194,195], under-represented regions and vegetation types[196] (Fig. 1d,e), scale mismatches[24], satellite and meteorological data errors, and limitations in upscaling methods[121,136,145]. The limitations of upscaled fluxes include infrequent updates, coarse spatial resolution, lack of uncertainty estimates and gaps in controlling factors, as well as substantial room for improvement in capturing interannual variability and trends[30,121].

Interpreting satellite-based vegetation products

EC measurements have been instrumental in interpreting satellite-based vegetation indices and retrievals, particularly in understanding their relations with carbon fluxes. The relations between vegetation indices and CO_2 exchange were first examined in the early and middle 1990s[10,11] (Fig. 1). EC measurements have helped evaluate how numerous vegetation indices, such as the normalized difference vegetation index[10,11], the photochemical reflectance index[197], the enhanced vegetation index[198] and near-infrared reflectance of terrestrial vegetation[199], relate to ecosystem CO_2 exchange. Although some indices are considered superior to others — such as enhanced vegetation index and near-infrared reflectance of terrestrial vegetation outperforming the normalized difference vegetation index — there is no consensus on which performs best[200].

EC data helped reveal that satellite-derived land surface temperature was nonlinearly correlated with RECO[201]. EC data also helped researchers find that solar-induced chlorophyll fluorescence measured

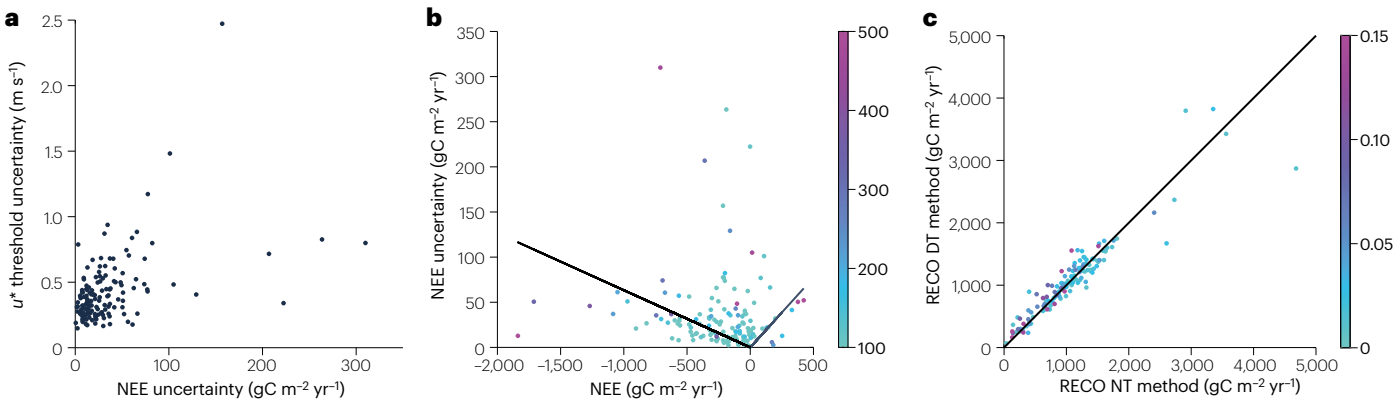

Fig. 5 | Uncertainty of annual carbon fluxes measured by the eddy covariance technique. a, The relationship between net ecosystem exchange (NEE) uncertainty as the interquartile range (IQR) of annual NEE (which results mainly from uncertainty in the u^* (friction velocity) threshold) and u^* threshold uncertainty (which is calculated as the ratio between the IQR of the u^* threshold and the median threshold across sites). The correlation between the two uncertainties is low ($R^2 = 0.2$), highlighting the absence of a simple, direct relationship between them and underscoring the site-specific nature of this uncertainty. **b**, The relationship between annual NEE and the NEE uncertainty as IQR of annual NEE across sites. The colour indicates the uncertainty in partitioning ecosystem respiration (RECO) as the difference between the two partitioning methods: night-time (NT) and daytime (DT). There is not a clear relation between NEE values and their uncertainty or with the uncertainty in RECO. **c**, The relationship between the two RECO estimates based on the NT and DT methods across sites. The colour indicates the uncertainty in NEE with respect to average RECO calculated as the ratio between the NEE uncertainty (as reported in panel **a**) and the average RECO. Data are based on the FLUXNET2015 database[20]. Together, these panels illustrate the complexity and site dependence of uncertainty in eddy covariance-derived annual carbon fluxes.

by satellites exhibits a strong linear relationship with photosynthesis and is a better indicator of GPP than vegetation indices[202–206]. In addition, the ratio of solar-induced chlorophyll fluorescence based on OCO-3 and ET estimated from ECOSTRESS offers a satellite-based measure of ecosystem WUE[1], and can monitor diurnal variations of plant water use[207].

Evaluating satellite-based flux products

EC data have been widely used to evaluate satellite-based GPP and ET products at daily or longer timescales. For example, the global Moderate Resolution Imaging Spectroradiometer (MODIS) GPP product[208] was first evaluated with GPP at the 12 AmeriFlux sites[209]. The MODIS ET product was validated in North America and Australia using the AmeriFlux and OzFlux data[210,211]. EC data are now routinely used to evaluate satellite-based GPP[212–214], NEE[148,214,215] and ET[216,217] products. The overall similarities, along with the relatively small discrepancies in spatial patterns, seasonal cycles and interannual variations of GPP between the eight satellite-based products and the five machine learning-upscaled products indicate both high performance of the satellite-based products and potential for improvement (Fig. 6). Since 2020, flux tower data have also been used to evaluate satellite-derived subdaily carbon[1,166,218] and water[217] flux estimates. Measurements from EC sites have also contributed to the validation of other satellite-derived products, such as shortwave solar radiation[219,220], PAR[219,221], longwave radiation[222,223], albedo[224,225] and phenology[226–228] (Supplementary Note 9). These satellite-derived products are often used in carbon and water cycling studies.

Benchmarking models

EC measurements have helped evaluate terrestrial biosphere models and Earth system models since the mid-1990s[12–14] (Fig. 1) and are now routinely used to evaluate individual models[229–231] or model ensembles[232–234]. Upscaled EC data have been widely used to evaluate terrestrial biosphere models[180,235] and Earth system models[236,237] at regional to global scales. Upscaled EC data confirm the value of such modelling studies, while also highlighting areas for model improvement. For example, the ensemble mean GPP from 21 process-based models exhibit similar spatial patterns, seasonal cycles and interannual variations to six upscaled GPP products based on machine learning. However, with relatively large differences in magnitude and a larger spread among models, this ensemble mean reflects both good performance of these process-based models and room for improvement (Fig. 6).

Upscaled flux products have also been used for evaluating atmospheric inversions[153,238,239]. For example, NEE upscaled from AmeriFlux data[158] agreed relatively well with inverted carbon fluxes at the subcontinental scale[238]. Seasonal variations in upscaled NEE were consistent with GOSAT-based inversion in mid- and high-latitude regions, with a large discrepancy in tropical regions[153]. These two types of estimates, however, still exhibit discrepancies that need to be reconciled.

Improving terrestrial biosphere models

EC measurements are also widely used to optimize parameters in LUE[147,240] and terrestrial biosphere models[15,241] with model–data fusion techniques to improve model performance. Parameter optimization with EC data can not only improve the performance of LUE models[213,240,242] but also lead to uncertainty estimates to regional fluxes[148]. Flux measurements were first used to estimate parameters of terrestrial biosphere models and land surface models in 2001[15]. Following this work, many studies used flux measurements from a single site or multiple sites to optimize uncertain parameters in these models[243–245]. EC measurements and upscaled data can also help identify model deficiencies and inform model improvement, contributing to improvement of process representation[246–248]. For example, the evaluation of the Community Land Model with EC measurements and upscaled data led to improvement of photosynthesis[248] and subsurface hydrological processes[246].

Summary and future perspectives

The global network of EC flux sites represents one of the largest and longest biogeochemical and geophysical experiments. These EC measurements and the resulting upscaled flux products have advanced research on the terrestrial carbon and water cycles by improving understanding of land–atmosphere carbon and water exchanges from the ecosystem to the global scale. They have also been foundational in evaluating and interpreting satellite-derived products, and benchmarking and improving terrestrial biosphere models, land surface models and Earth system models. Building on these achievements, EC measurements coordinated by regional flux networks and FLUXNET, along with associated upscaled data and their use in research, are poised to expand and evolve further, offering new opportunities to deepen our understanding of the terrestrial carbon and water cycles.

Although many EC sites have been established, additional sites are still needed in under-represented regions to improve network representativeness. Even an extensive network cannot capture the full range of variations in vegetation, climate, soil, disturbance history and management. Thus, ecological questions often require ancillary data such as LAI, biomass, soil properties, soil respiration and biodiversity that are difficult and time consuming to collect. One strategy to address these needs is to support two complementary networks: one composed of detailed anchor sites with comprehensive, long-term measurements that serve as baselines for process understanding and model development; and another, broadly distributed network collecting fluxes and key meteorological variables across diverse ecological and environmental conditions for upscaling. Both networks could be supported by coordinated data centres for processing and distribution[249].

Data sharing remains a challenge, and promoting open access such as mandating public data deposition for journal publication, grant funding and talent programmes would substantially increase data availability in regions such as China, South America and Africa. Proper citation of openly shared datasets and integration of citation metrics into researcher and institution evaluations would further incentivize sharing. Moreover, the latencies of EC measurements — the time lag between data collection and release — can be up to a few years. Therefore, making measurements, particularly gap filled and partitioned data, available in near real time is a priority. Establishing coordination among regional networks with direct contact to site teams to organize rapid standardized data processing and distribution could make data available in near real time. Publishing an annual joint data article co-authored by data contributors from the previous year could incentivize the timely release of new measurements.

Upscaling EC measurements to regional or global scales should be improved by introducing physical constraints, and ecological principles should be introduced to ensure mass balance and better capture interannual variability in fluxes. For example, NEE and its constituent fluxes, GPP and RECO, are typically upscaled separately and, owing to uncertainties, often do not satisfy their mass balance relationship (NEE = RECO − GPP).

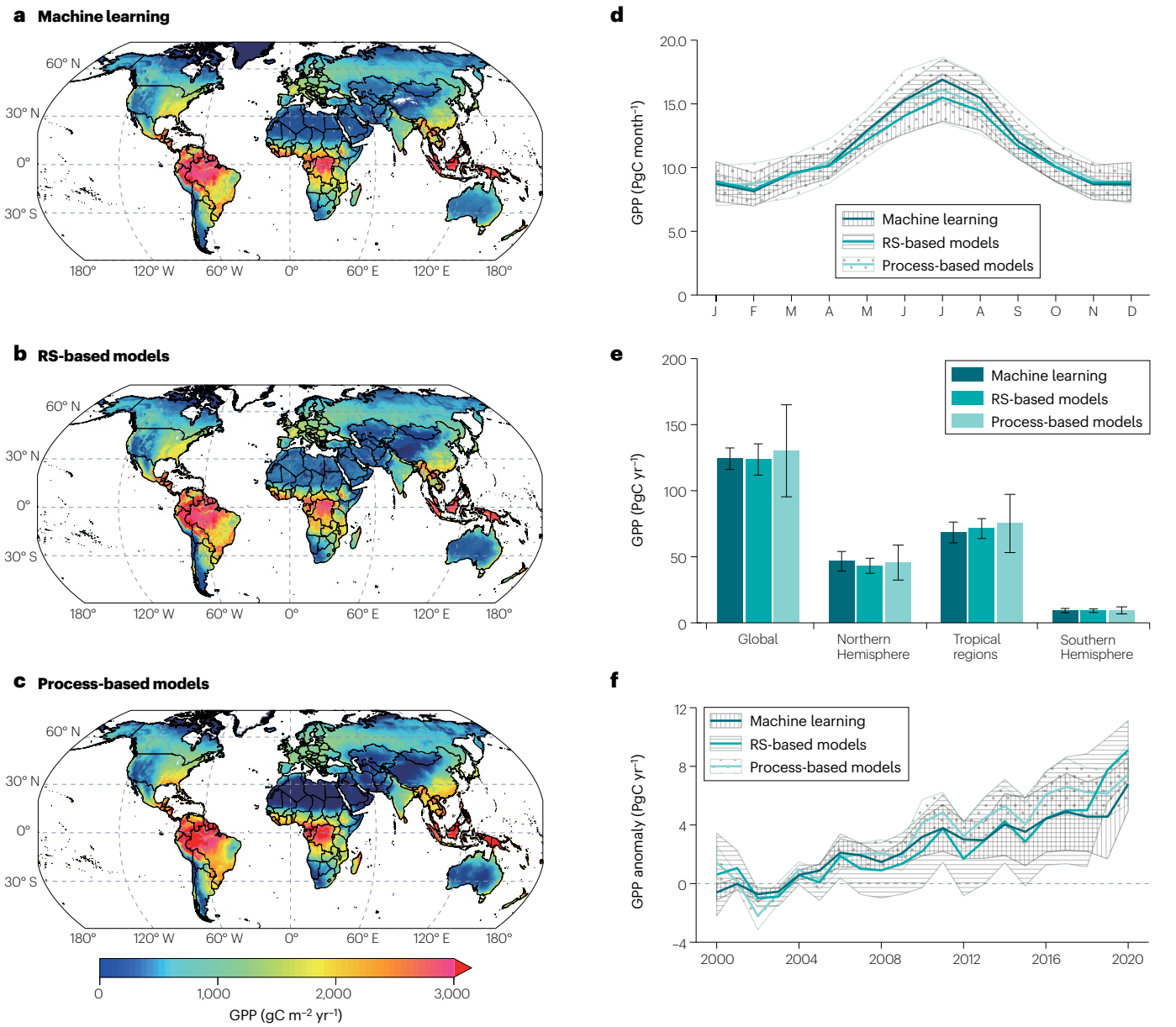

Fig. 6 | Evaluating the annual GPP of satellite-based products and process-based models. a–**c**, Annual gross primary production (GPP) estimated as the multi-model mean based on machine learning (**a**), remote sensing (RS)-based models (**b**) and process-based models included in the TRENDY experiment (version 12) (**c**). Annual GPP is calculated as multi-model mean for the 2000–2020 period. The model details are described in Supplementary Table 3. **d**, The monthly variation in global GPP estimated by multi-model mean of the three different approaches. The standard deviation across models is shown as shade. **e**, The mean annual total GPP and its standard deviations across the globe, Northern Hemisphere (>22.5° N) tropical regions (22.5° N to 22.5° S) and Southern Hemisphere (<22.5° S) based on the three approaches. **f**, The interannual variations in global GPP and their standard deviations for the three approaches. Anomalies were calculated using the values over 2000–2004 as the baseline (see Supplementary Figs. 7 and 8 for the spread in seasonal cycles and the annual totals of GPP among models and products used in each type of approach). The upscaled flux products provide a valuable benchmark for assessing spatial patterns, seasonal dynamics, annual totals, and long-term trends in fluxes derived from satellite-based models and process-based models.

In addition, advanced machine learning and artificial intelligence techniques, such as deep learning architectures and foundation models, should be applied to better represent ecosystem behaviour, memory and legacy effects of environmental stresses. In particular, such models should focus on capturing nonlinear, lagged and legacy effects that characterize long-term ecosystem dynamics that are omitted from existing machine learning approaches. For instance, emerging deep learning architectures can integrate temporal dependencies, such as Long Short-Term Memory and Transformer. Foundation models, pre-trained on large and diverse datasets, could

also enhance EC measurement upscaling by improving spatial and temporal generalization and facilitating transfer learning across regions. Finally, integrating machine learning and process-based modelling could potentially leverage the strengths of both data-driven and mechanistic methods to achieve enhanced accuracy and physical consistency in flux estimates.

Emerging satellite observations could be better leveraged to improve the upscaling of EC measurements. For instance, LiDAR,

Glossary

Disturbance
Events that alter ecosystem carbon and water fluxes, such as fire, logging, hurricanes and insect outbreaks.

Earth system models
Comprehensive, computer-based models that simulate coupled interactions among the atmosphere, oceans, land and biosphere, including carbon, water and energy cycles.

Ecosystem assimilation
The amount of atmospheric CO_2 absorbed by plants through photosynthesis; equivalent to gross primary production.

Ecosystem respiration
The total release of CO_2 from an ecosystem to the atmosphere through autotrophic and heterotrophic respiration.

Eddy covariance
(EC) A micrometeorological technique that directly and continuously measures the exchange of gases, energy, and momentum between ecosystems and the atmosphere at high frequency.

Enhanced vegetation index
A remote-sensing vegetation index indicative of canopy greenness and photosynthetic activity, designed to minimize atmospheric and soil background effects.

Evaporative fraction
The ratio of latent heat flux to the sum of latent and sensible heat fluxes, which indicates surface energy partitioning and plant water status.

Evapotranspiration
(ET) The sum of evaporation from canopy, soil and water surfaces plus transpiration from plants, which can be calculated from latent heat flux measurements.

Explanatory variables
Independent variables or predictors used in statistical or machine learning analyses.

Fraction of photosynthetically active radiation
The proportion of photosynthetically active radiation absorbed by vegetation canopies.

Friction velocity
(u^*) A key parameter quantifying the intensity of atmospheric turbulence, used to filter out low-turbulence flux data, particularly at night.

Gap filled
The process of estimating missing eddy covariance measurements due to instrument failures or data quality issues.

Gross primary production
(GPP) The total amount of atmospheric CO_2 fixed by an ecosystem through photosynthesis.

Hysteresis
Dependence of a system's response on its prior states or history, leading to lagged or looped input–output relationships.

Latent heat flux
The energy flux associated with evapotranspiration, representing water loss from the surface and a major component of the surface energy budget.

Leaf area index
(LAI) The total one-sided green leaf area per unit ground surface area.

Leaf senescence
The ageing and programmed degradation of leaves, involving nutrient remobilization and eventual leaf death.

Light-use efficiency
(LUE) The efficiency with which plants convert absorbed light into carbon gain through photosynthesis.

Machine learning
Algorithms that identify patterns in data and make predictions or decisions, as part of artificial intelligence.

Near-infrared reflectance of terrestrial vegetation
A remote sensing vegetation index calculated as the product of near-infrared reflectance and the normalized difference vegetation index, used as a proxy for canopy photosynthetic activity.

Net ecosystem exchange
(NEE) The net flux of CO_2 between an ecosystem and the atmosphere, where negative values indicate ecosystem carbon uptake and positive values indicate carbon release into the atmosphere.

Normalized difference vegetation index
A remote sensing vegetation index calculated from the contrast in reflectance between red and near-infrared bands, indicative of canopy greenness and photosynthetic activity.

Photochemical reflectance index
A remote-sensing vegetation index indicating changes in photosynthetic light-use efficiency.

Photosynthetically active radiation
(PAR) Incoming solar radiation in the wavelength range of 400–700 nm used for photosynthesis.

Sensible heat flux
Energy flux that warms or cools the air without a phase change.

Solar-induced chlorophyll fluorescence
The faint energy flux re-emitted by chlorophyll during photosynthesis, providing a direct proxy for photosynthetic activity and gross primary production.

Stomatal conductance
The rate at which CO_2 enters and water vapour exits a leaf through stomata, reflecting plant water–carbon exchange regulation.

Terrestrial biosphere models
Mechanistic, computer-based models that represent the processes of carbon, water and energy exchanges between the terrestrial biosphere and the atmosphere.

Tower footprint
The upwind surface area contributing to the fluxes measured by an eddy covariance tower.

Upscaling
The process of extending site-level measurements, such as eddy covariance fluxes, to regional or global scales using machine learning or modelling combined with satellite and climate data.

Vapour pressure deficit
(VPD) The difference between the saturation and actual vapour pressure of water in the air; a key driver of transpiration.

Water-use efficiency
(WUE) The ratio of carbon gain through photosynthesis to water loss via transpiration, representing how efficiently plants or ecosystems use water.

hyperspectral, solar-induced chlorophyll fluorescence, CubeSat, thermal and geostationary data could help provide additional context and constraints related to disturbance, nutrient limitation, CO_2 fertilization, substrate availability, ecosystem structure, biodiversity, high spatial resolution, and diurnal dynamics.

Future improvements in upscaled flux products can be made in several key areas. First, developing near real-time products with shorter latencies — now feasible given availability of satellite and meteorological reanalysis datasets with 1–2-month latencies — will better serve time-sensitive applications. Second, finer-resolution (for example, 30 m or 10 m) flux estimates enabled by high-resolution satellite data and cloud computing would benefit numerous studies. Third, on-demand web-based tools on cloud-computing platforms for generating fine-resolution flux estimates for any region and time would be valuable for many applications. Finally, providing per-pixel uncertainty estimates accounting for various sources of uncertainty would enhance usability and user confidence.

FLUXNET data will continue to help address fundamental science questions and goals of climate and carbon cycle research programmes. For example, one fundamental question relates to the capacity of the global terrestrial ecosystem to absorb carbon via photosynthesis. FLUXNET data are likely to help elucidate whether high global GPP estimates (170–200 PgC yr^{-1})[250] are theoretically possible. Schmidt Sciences' Virtual Institute for the Carbon Cycle aims to achieve an accuracy of 0.1 $PgCO_2$ yr^{-1} in global carbon budget measurements. Although the EC technique is most accurate for continuously measuring ecosystem-level carbon exchange[251], it still faces considerable uncertainty, raising doubts about the feasibility of this target. EC data are increasingly crucial for climate mitigation, carbon trading and nature-based solutions[252,253], especially with the development of affordable, robust EC gas analysers.

The future of the regional networks of EC sites, their coordination under the FLUXNET umbrella, and their evolution through advancements in both sensor and data processing, as well as international collaborations among site personnel and data users, will play a pivotal role in shaping the continued importance of flux data moving forwards. These data hold the potential to support a broad spectrum of studies and applications across various spatial and temporal scales — particularly when integrated with other data types and methodologies — yet much of this potential remains untapped. EC data are expected to continue to greatly advance terrestrial carbon and water cycle research in decades to come. Realizing this potential, however, hinges on the adoption and implementation of a fair, open and near real-time data-sharing policy by all stakeholders, a key challenge that FLUXNET will need to address to ensure future success.

Published online: 20 November 2025

References

1. Xiao, J. F., Fisher, J. B., Hashimoto, H., Ichii, K. & Parazoo, N. C. Emerging satellite observations for diurnal cycling of ecosystem processes. *Nat. Plants* **7**, 877–887 (2021).
2. Tucci, M. L. S., Erismann, N. M., Machado, E. C. & Ribeiro, R. V. Diurnal and seasonal variation in photosynthesis of peach palms grown under subtropical conditions. *Photosynthetica* **48**, 421–429 (2010).
3. Koch, G. W., Amthor, J. S. & Goulden, M. L. Diurnal patterns of leaf photosynthesis, conductance and water potential at the top of a lowland rain-forest canopy in Cameroon — measurements from the Radeau-Des-Cimes. *Tree Physiol.* **14**, 347–360 (1994).
4. Wofsy, S. C. et al. Net exchange of CO_2 in a midlatitude forest. *Science* **260**, 1314–1317 (1993).
5. Baldocchi, D. et al. FLUXNET: a new tool to study the temporal and spatial variability of ecosystem-scale carbon dioxide, water vapor, and energy flux densities. *Bull. Am. Meteorol. Soc.* **82**, 2415–2434 (2001).
6. Desjardins, R. L. Technique to measure CO_2 exchange under field conditions. *Int. J. Biometeorol.* **18**, 76–83 (1974).
7. Desjardins, R. L. & Lemon, E. R. Limitations of an eddy covariance technique for the determination of the carbon dioxide and sensible heat fluxes. *Bound. Layer Meteorol.* **5**, 475–488 (1974).
8. Ohtaki, E. Application of an infrared carbon-dioxide and humidity instrument to studies of turbulent transport. *Bound. Layer Meteorol.* **29**, 85–107 (1984).
9. Desjardins, R. L. Carbon-dioxide budget of maize. *Agric. For. Meteorol.* **36**, 29–41 (1985).
10. Whiting, G. J., Bartlett, D. S., Fan, S. M., Bakwin, P. S. & Wofsy, S. C. Biosphere atmosphere CO_2 exchange in tundra ecosystems — community characteristics and relationships with multispectral surface reflectance. *J. Geophys. Res.* **97**, 16671–16680 (1992).
11. Gamon, J. A. et al. Relationships between NDVI, canopy structure, and photosynthesis in 3 Californian vegetation types. *Ecol. Appl.* **5**, 28–41 (1995).
12. Waring, R. H. et al. Scaling gross ecosystem production at Harvard Forest with remote sensing: a comparison of estimates from a constrained quantum-use efficiency model and eddy correlation. *Plant Cell Environ.* **18**, 1201–1213 (1995).
13. Amthor, J. S., Goulden, M. L., Munger, J. W. & Wofsy, S. C. Testing a mechanistic model of forest-canopy mass and energy exchange using eddy correlation: carbon dioxide and ozone uptake by a mixed oak-maple stand. *Aust. J. Plant. Physiol.* **21**, 623–651 (1994).
14. Baldocchi, D. D. & Harley, P. C. Scaling carbon dioxide and water vapour exchange from leaf to canopy in a deciduous forest. II. Model testing and application. *Plant Cell Environ.* **18**, 1157–1173 (1995).
15. Wang, Y. P., Leuning, R., Cleugh, H. A. & Coppin, P. A. Parameter estimation in surface exchange models using nonlinear inversion: how many parameters can we estimate and which measurements are most useful? *Glob. Change Biol.* **7**, 495–510 (2001).
16. Urbanski, S. et al. Factors controlling CO_2 exchange on timescales from hourly to decadal at Harvard Forest. *J. Geophys. Res.* **112**, G02020 (2007).
17. Dunn, A. L., Barford, C. C., Wofsy, S. C., Goulden, M. L. & Daube, B. C. A long-term record of carbon exchange in a boreal black spruce forest: means, responses to interannual variability, and decadal trends. *Glob. Change Biol.* **13**, 577–590 (2007).
18. Aubinet, M. et al. Estimates of the annual net carbon and water exchange of forests: the EUROFLUX methodology. *Adv. Ecol. Res.* **30**, 113–175 (1999).
19. Baldocchi, D. D. et al. Predicting the onset of net carbon uptake by deciduous forests with soil temperature and climate data: a synthesis of FLUXNET data. *Int. J. Biometeorol.* **49**, 377–387 (2005).
20. Pastorello, G. et al. The FLUXNET2015 dataset and the ONEFlux processing pipeline for eddy covariance data. *Sci. Data* **7**, 225 (2020).
21. Beer, C. et al. Temporal and among-site variability of inherent water use efficiency at the ecosystem level. *Glob. Biogeochem. Cycle* https://doi.org/10.1029/2008GB003233 (2009).
22. Luyssaert, S. et al. Old-growth forests as global carbon sinks. *Nature* **455**, 213–215 (2008).
23. Papale, D. & Valentini, A. A new assessment of European forests carbon exchanges by eddy fluxes and artificial neural network spatialization. *Glob. Change Biol.* **9**, 525–535 (2003).
24. Xiao, J. F. et al. Estimation of net ecosystem carbon exchange for the conterminous United States by combining MODIS and AmeriFlux data. *Agric. For. Meteorol.* **148**, 1827–1847 (2008).
25. Jung, M., Reichstein, M. & Bondeau, A. Towards global empirical upscaling of FLUXNET eddy covariance observations: validation of a model tree ensemble approach using a biosphere model. *Biogeosciences* **6**, 2001–2013 (2009).
26. Li, F. et al. Global water use efficiency saturation due to increased vapor pressure deficit. *Science* **381**, 672–677 (2023).
27. Baldocchi, D. D. How eddy covariance flux measurements have contributed to our understanding of global change biology. *Glob. Change Biol.* **26**, 242–260 (2020).
28. Baldocchi, D., Chu, H. S. & Reichstein, M. Inter-annual variability of net and gross ecosystem carbon fluxes: a review. *Agric. For. Meteorol.* **249**, 520–533 (2018).
29. Xiao, J. et al. Remote sensing of the terrestrial carbon cycle: a review of advances over 50 years. *Remote Sens. Environ.* **233**, 111383 (2019).
30. Jung, M. et al. Scaling carbon fluxes from eddy covariance sites to globe: synthesis and evaluation of the FLUXCOM approach. *Biogeosciences* **17**, 1343–1365 (2020).
31. Baldocchi, D. Breathing of the terrestrial biosphere: lessons learned from a global network of carbon dioxide flux measurement systems. *Aust. J. Bot.* **56**, 1–26 (2008).
32. Goulden, M. L. et al. Diel and seasonal patterns of tropical forest CO_2 exchange. *Ecol. Appl.* **14**, S42–S54 (2004).
33. San-José, J., Montes, R. & Nikonova, N. Diurnal patterns of carbon dioxide, water vapour, and energy fluxes in pineapple *Ananas comosus* (L) Merr. cv. Red Spanish field using eddy covariance. *Photosynthetica* **45**, 370–384 (2007).
34. Paul-Limoges, E. et al. Partitioning evapotranspiration with concurrent eddy covariance measurements in a mixed forest. *Agric. For. Meteorol.* **280**, 107786 (2020).
35. Xu, H., Xiao, J. F. & Zhang, Z. Q. Heatwave effects on gross primary production of northern mid-latitude ecosystems. *Environ. Res. Lett.* **15**, 074027 (2020).
36. Lin, C. J. et al. Evaluation and mechanism exploration of the diurnal hysteresis of ecosystem fluxes. *Agric. For. Meteorol.* **278**, 107642 (2019).
37. Zheng, H., Wang, Q. F., Zhu, X. J., Li, Y. N. & Yu, G. R. Hysteresis responses of evapotranspiration to meteorological factors at a diel timescale: patterns and causes. *PLoS ONE* **9**, e98857 (2014).
38. Kwon, H., Pendall, E., Ewers, B. E., Cleary, M. & Naithani, K. Spring drought regulates summer net ecosystem CO_2 exchange in a sagebrush-steppe ecosystem. *Agric. For. Meteorol.* **148**, 381–391 (2008).

39. Tenhunen, J. D., Lange, O. L., Gebel, J., Beyschlag, W. & Weber, J. A. Changes in photosynthetic capacity, carboxylation efficiency, and CO_2 compensation point associated with midday stomatal closure and midday depression of net CO_2 exchange of leaves of *Quercus suber*. *Planta* **162**, 193–203 (1984).
40. Nelson, J. A., Carvalhais, N., Migliavacca, M., Reichstein, M. & Jung, M. Water-stress-induced breakdown of carbon–water relations: indicators from diurnal FLUXNET patterns. *Biogeosciences* **15**, 2433–2447 (2018).
41. van Gorsel, E. et al. Carbon uptake and water use in woodlands and forests in southern Australia during an extreme heat wave event in the "Angry Summer" of 2012/2013. *Biogeosciences* **13**, 5947–5964 (2016).
42. Richardson, A. D. et al. Influence of spring and autumn phenological transitions on forest ecosystem productivity. *Philos. Trans. R. Soc. B* **365**, 3227–3246 (2010).
43. Chapin, F. S. et al. Reconciling carbon-cycle concepts, terminology, and methods. *Ecosystems* **9**, 1041–1050 (2006).
44. Chen, Z. et al. Covariation between gross primary production and ecosystem respiration across space and the underlying mechanisms: a global synthesis. *Agric. For. Meteorol.* **203**, 180–190 (2015).
45. Niu, S. L. et al. Temperature responses of ecosystem respiration. *Nat. Rev. Earth Environ.* **5**, 559–571 (2024).
46. Zhang, Q. et al. Water limitation regulates positive feedback of increased ecosystem respiration. *Nat. Ecol. Evol.* **8**, 1870–1876 (2024).
47. Schwinning, S., Sala, O. E., Loik, M. E. & Ehleringer, J. R. Thresholds, memory, and seasonality: understanding pulse dynamics in arid/semi-arid ecosystems. *Oecologia* **141**, 191–193 (2004).
48. Baldocchi, D., Tang, J. W. & Xu, L. K. How switches and lags in biophysical regulators affect spatial-temporal variation of soil respiration in an oak-grass savanna. *J. Geophys. Res.* **111**, G02008 (2006).
49. Jarvis, P. et al. Drying and wetting of Mediterranean soils stimulates decomposition and carbon dioxide emission: the "Birch effect". *Tree Physiol.* **27**, 929–940 (2007).
50. Rutledge, S., Campbell, D. I., Baldocchi, D. & Schipper, L. A. Photodegradation leads to increased carbon dioxide losses from terrestrial organic matter. *Glob. Change Biol.* **16**, 3065–3074 (2010).
51. Kannenberg, S. A., Anderegg, W. R. L., Barnes, M. L., Dannenberg, M. P. & Knapp, A. K. Dominant role of soil moisture in mediating carbon and water fluxes in dryland ecosystems. *Nat. Geosci.* **17**, 38–43 (2024).
52. Roby, M. C., Scott, R. L. & Moore, D. J. P. High vapor pressure deficit decreases the productivity and water use efficiency of rain-induced pulses in semiarid ecosystems. *J. Geophys. Res.* **125**, e2020JG005665 (2020).
53. Noormets, A. et al. Response of carbon fluxes to drought in a coastal plain loblolly pine forest. *Glob. Change Biol.* **16**, 272–287 (2010).
54. Baldocchi, D., Ma, S. Y. & Verfaillie, J. On the inter- and intra-annual variability of ecosystem evapotranspiration and water use efficiency of an oak savanna and annual grassland subjected to booms and busts in rainfall. *Glob. Change Biol.* **27**, 359–375 (2021).
55. Ruehr, S. et al. Ecosystem groundwater use enhances carbon assimilation and tree growth in a semi-arid oak savanna. *Agric. For. Meteorol.* **342**, 109725 (2023).
56. Pereira, J. S. et al. Net ecosystem carbon exchange in three contrasting Mediterranean ecosystems — the effect of drought. *Biogeosciences* **4**, 791–802 (2007).
57. van der Woude, A. M. et al. Temperature extremes of 2022 reduced carbon uptake by forests in Europe. *Nat. Commun.* **14**, 6218 (2023).
58. Schwalm, C. R. et al. Assimilation exceeds respiration sensitivity to drought: a FLUXNET synthesis. *Glob. Change Biol.* **16**, 657–670 (2010).
59. Miller, D. L. et al. Increased photosynthesis during spring drought in energy-limited ecosystems. *Nat. Commun.* **14**, 7828 (2023).
60. Zhang, M. & Yuan, X. Rapid reduction in ecosystem productivity caused by flash droughts based on decade-long FLUXNET observations. *Hydrol. Earth Syst. Sci.* **24**, 5579–5593 (2020).
61. Otkin, J. A. et al. Flash droughts: a review and assessment of the challenges imposed by rapid-onset droughts in the United States. *Bull. Am. Meteorol. Soc.* **99**, 911–919 (2018).
62. Clark, K. L., Skowronski, N., Gallagher, M., Renninger, H. & Schäfer, K. Effects of invasive insects and fire on forest energy exchange and evapotranspiration in the New Jersey pinelands. *Agric. For. Meteorol.* **166**, 50–61 (2012).
63. Lu, W. Z. et al. Insect outbreaks have transient effects on carbon fluxes and vegetative growth but longer-term impacts on reproductive growth in a mangrove forest. *Agric. For. Meteorol.* **279**, 107747 (2019).
64. Knowles, J. F. et al. Bark beetle impacts on forest evapotranspiration and its partitioning. *Sci. Total Environ.* **880**, 163260 (2023).
65. Black, T. A. et al. Annual cycles of water vapour and carbon dioxide fluxes in and above a boreal aspen forest. *Glob. Change Biol.* **2**, 219–229 (1996).
66. Greco, S. & Baldocchi, D. D. Seasonal variations of CO_2 and water vapour exchange rates over a temperate deciduous forest. *Glob. Change Biol.* **2**, 183–197 (1996).
67. Valentini, R. et al. Seasonal net carbon dioxide exchange of a beech forest with the atmosphere. *Glob. Change Biol.* **2**, 199–207 (1996).
68. Budyko, M. *Climate and Life* (Academic Press, 1974).
69. Williams, C. A. et al. Climate and vegetation controls on the surface water balance: synthesis of evapotranspiration measured across a global network of flux towers. *Water Resour. Res.* **48**, W06523 (2012).
70. Wang, H. B., Li, X., Xiao, J. F. & Ma, M. G. Evapotranspiration components and water use efficiency from desert to alpine ecosystems in drylands. *Agric. For. Meteorol.* **298**, 108283 (2021).
71. Alton, P. B. How useful are plant functional types in global simulations of the carbon, water, and energy cycles? *J. Geophys. Res.* **116**, G01030 (2011).
72. Groenendijk, M. et al. Assessing parameter variability in a photosynthesis model within and between plant functional types using global Fluxnet eddy covariance data. *Agric. For. Meteorol.* **151**, 22–38 (2011).
73. Zhou, H. et al. Distinguishing the main climatic drivers to the variability of gross primary productivity at global FLUXNET sites. *Environ. Res. Lett.* **18**, 124007 (2023).
74. Churkina, G., Schimel, D., Braswell, B. H. & Xiao, X. M. Spatial analysis of growing season length control over net ecosystem exchange. *Glob. Change Biol.* **11**, 1777–1787 (2005).
75. Xiao, J. F. et al. Carbon fluxes, evapotranspiration, and water use efficiency of terrestrial ecosystems in China. *Agric. For. Meteorol.* **182-183**, 76–90 (2013).
76. Wolf, S. et al. Warm spring reduced carbon cycle impact of the 2012 US summer drought. *Proc. Natl Acad. Sci. USA* **113**, 5880–5885 (2016).
77. Law, B. E. et al. Environmental controls over carbon dioxide and water vapor exchange of terrestrial vegetation. *Agric. For. Meteorol.* **113**, 97–120 (2002).
78. Baldocchi, D. & Penuelas, J. The physics and ecology of mining carbon dioxide from the atmosphere by ecosystems. *Glob. Change Biol.* **25**, 1191–1197 (2019).
79. Cowan, I. R. & Farquhar, G. D. Stomatal function in relation to leaf metabolism and environment: stomatal function in the regulation of gas exchange. *Symp. Soc. Exp. Biol.* **31**, 471–505 (1977).
80. Biederman, J. A. et al. CO_2 exchange and evapotranspiration across dryland ecosystems of southwestern North America. *Glob. Change Biol.* **23**, 4204–4221 (2017).
81. Anderson-Teixeira, K. J., Delong, J. P., Fox, A. M., Brese, D. A. & Litvak, M. E. Differential responses of production and respiration to temperature and moisture drive the carbon balance across a climatic gradient in New Mexico. *Glob. Change Biol.* **17**, 410–424 (2011).
82. Ueyama, M., Iwata, H. & Harazono, Y. Autumn warming reduces the CO_2 sink of a black spruce forest in interior Alaska based on a nine-year eddy covariance measurement. *Glob. Change Biol.* **20**, 1161–1173 (2013).
83. Saigusa, N., Yamamoto, S., Murayama, S. & Kondo, H. Inter-annual variability of carbon budget components in an AsiaFlux forest site estimated by long-term flux measurements. *Agric. For. Meteorol.* **134**, 4–16 (2005).
84. Zha, T. et al. Interannual variation of evapotranspiration from forest and grassland ecosystems in western Canada in relation to drought. *Agric. For. Meteorol.* **150**, 1476–1484 (2010).
85. Geddes, J. A. et al. Net ecosystem exchange of an uneven-aged managed forest in central Ontario, and the impact of a spring heat wave event. *Agric. For. Meteorol.* **198-199**, 105–115 (2014).
86. Herbst, M., Mund, M., Tamrakar, R. & Knohl, A. Differences in carbon uptake and water use between a managed and an unmanaged beech forest in central Germany. *For. Ecol. Manage.* **355**, 101–108 (2015).
87. Flanagan, L. B., Wever, L. A. & Carlson, P. J. Seasonal and interannual variation in carbon dioxide exchange and carbon balance in a northern temperate grassland. *Glob. Change Biol.* **8**, 599–615 (2002).
88. Jongen, M., Pereira, J. S., Aires, L. M. I. & Pio, C. A. The effects of drought and timing of precipitation on the inter-annual variation in ecosystem-atmosphere exchange in a Mediterranean grassland. *Agric. For. Meteorol.* **151**, 595–606 (2011).
89. Gu, L. H. et al. Advantages of diffuse radiation for terrestrial ecosystem productivity. *J. Geophys. Res.* **107**, 4050 (2002).
90. Burba, G. G. & Verma, S. B. Seasonal and interannual variability in evapotranspiration of native tallgrass prairie and cultivated wheat ecosystems. *Agric. For. Meteorol.* **135**, 190–201 (2005).
91. Saleska, S. R. et al. Carbon in amazon forests: unexpected seasonal fluxes and disturbance-induced losses. *Science* **302**, 1554–1557 (2003).
92. Ciais, P. et al. Europe-wide reduction in primary productivity caused by the heat and drought in 2003. *Nature* **437**, 529–533 (2005).
93. Amiro, B. D. et al. Ecosystem carbon dioxide fluxes after disturbance in forests of North America. *J. Geophys. Res.* **115**, G00K02 (2010).
94. Heliasz, M. et al. Quantification of C uptake in subarctic birch forest after setback by an extreme insect outbreak. *Geophys. Res. Lett.* **38**, L01704 (2011).
95. Kenney, G. et al. Hurricane Michael altered the structure and function of longleaf pine woodlands. *J. of Geophys. Res. Biogeosci.* **126**, e2021JG006452 (2021).
96. Hirano, T., Suzuki, K. & Hirata, R. Energy balance and evapotranspiration changes in a larch forest caused by severe disturbance during an early secondary succession. *Agric. For. Meteorol.* **232**, 457–468 (2017).
97. Amiro, B. D. et al. Carbon, energy and water fluxes at mature and disturbed forest sites, Saskatchewan, Canada. *Agric. For. Meteorol.* **136**, 237–251 (2006).
98. Odum, E. P. The strategy of ecosystem development. *Science* **164**, 262–270 (1969).
99. Kira, T. & Shidei, T. Primary production and turnover of organic matter in different forest ecosystems of the western Pacific. *Jpn J. Ecol.* **17**, 70–87 (1967).
100. Nabuurs, G. J. et al. First signs of carbon sink saturation in European forest biomass. *Nat. Clim. Change* **3**, 792–796 (2013).
101. Zhan, C. H. et al. Estimating the CO_2 fertilization effect on extratropical forest productivity from flux-tower observations. *J. Geophys. Res.* **129**, e2023JG007910 (2024).
102. Ueyama, M. et al. Inferring CO_2 fertilization effect based on global monitoring land-atmosphere exchange with a theoretical model. *Environ. Res. Lett.* **15**, 084009 (2020).
103. Keenan, T. F. et al. Increase in forest water-use efficiency as atmospheric carbon dioxide concentrations rise. *Nature* **499**, 324–327 (2013).

104. Wang, S. H. et al. Recent global decline of CO_2 fertilization effects on vegetation photosynthesis. *Science* **370**, 1295–1300 (2020).
105. Wang, G. et al. No widespread decline in canopy conductance under elevated atmospheric CO_2. *Agric. For. Meteorol.* **371**, 110649 (2025).
106. Mason, R. E. et al. Evidence, causes, and consequences of declining nitrogen availability in terrestrial ecosystems. *Science* **376**, 261 (2022).
107. Wang, X. F. et al. No trends in spring and autumn phenology during the global warming hiatus. *Nat. Commun.* **10**, 2389 (2019).
108. Xu, S. Q. et al. Response of ecosystem productivity to high vapor pressure deficit and low soil moisture: lessons learned from the global eddy-covariance observations. *Earths Future* **11**, e2022EF003252 (2023).
109. Massmann, A., Gentine, P. & Lin, C. J. When does vapor pressure deficit drive or reduce evapotranspiration? *J. Adv. Model. Earth Syst.* **11**, 3305–3320 (2019).
110. Yuan, W. P. et al. Increased atmospheric vapor pressure deficit reduces global vegetation growth. *Sci. Adv.* **5**, eaax1396 (2019).
111. Liu, P. et al. Seasonal warming responses of the carbon dioxide sink from northern forests are sensitive to stand age. *Commun. Earth Environ.* **6**, 43 (2025).
112. Liu, R., Cieraad, E., Li, Y. & Ma, J. Precipitation pattern determines the inter-annual variation of herbaceous layer and carbon fluxes in a phreatophyte-dominated desert ecosystem. *Ecosystems* **19**, 601–614 (2016).
113. Xue, B. et al. Global evapotranspiration hiatus explained by vegetation structural and physiological controls. *Ecol. Eng.* **158**, 106046 (2020).
114. Schmid, H. P. Source areas for scalars and scalar fluxes. *Bound. Layer Meteor.* **67**, 293–318 (1994).
115. Xiao, J. F., Chen, J. Q., Davis, K. J. & Reichstein, M. Advances in upscaling of eddy covariance measurements of carbon and water fluxes. *J. Geophys. Res.* **117**, G00J01 (2012).
116. Xu, T. et al. Evaluating different machine learning methods for upscaling evapotranspiration from flux towers to the regional scale. *J. Geophys. Res. Atmos.* **123**, 8674–8690 (2018).
117. Zhao, Y., Dong, H., Huang, W., He, S. & Zhang, C. Seamless terrestrial evapotranspiration estimation by machine learning models across the contiguous United States. *Ecol. Indic.* **165**, 112203 (2024).
118. Zhang, L., Xiao, J. F., Zheng, Y., Li, S. N. & Zhou, Y. Increased carbon uptake and water use efficiency in global semi-arid ecosystems. *Environ. Res. Lett.* **15**, 034022 (2020).
119. Jung, M. et al. The FLUXCOM ensemble of global land-atmosphere energy fluxes. *Sci. Data* **6**, 74 (2019).
120. Wang, Y. Y. et al. Persistent and enhanced carbon sequestration capacity of alpine grasslands on Earth's third pole. *Sci. Adv.* **9**, eade6875 (2023).
121. Xiao, J. F. et al. Data-driven diagnostics of terrestrial carbon dynamics over North America. *Agric. For. Meteorol.* **197**, 142–157 (2014).
122. Villarreal, S. & Vargas, R. Representativeness of FLUXNET sites across Latin America. *J. Geophys. Res. Biogeosci.* **126**, e2020JG006090 (2021).
123. Sulkava, M., Luyssaert, S., Zaehle, S. & Papale, D. Assessing and improving the representativeness of monitoring networks: the European flux tower network example. *J. Geophys. Res. Biogeosci.* **116**, G00J04 (2011).
124. Chu, H., Baldocchi, D. D., John, R., Wolf, S. & Reichstein, M. Fluxes all of the time? A primer on the temporal representativeness of FLUXNET. *J. Geophys. Res. Biogeosci.* **122**, 289–307 (2017).
125. Farquhar, G. D., Caemmerer, S. V. & Berry, J. A. A biochemical model of photosynthetic CO_2 assimilation in leaves of C_3 species. *Planta* **149**, 78–90 (1980).
126. Monteith, J. L. Solar radiation and productivity in tropical ecosystems. *J. Appl. Ecol.* **9**, 747–766 (1972).
127. Xiao, J. F. et al. A continuous measure of gross primary production for the conterminous United States derived from MODIS and AmeriFlux data. *Remote Sens. Environ.* **114**, 576–591 (2010).
128. Jung, M. et al. Global patterns of land–atmosphere fluxes of carbon dioxide, latent heat, and sensible heat derived from eddy covariance, satellite, and meteorological observations. *J. Geophys. Res.* **116**, G00J07 (2011).
129. Yao, Y. T. et al. A new estimation of China's net ecosystem productivity based on eddy covariance measurements and a model tree ensemble approach. *Agric. For. Meteorol.* **253**, 84–93 (2018).
130. Bu, J. & Xiao, J. Upscaling eddy covariance measurements of carbon and water fluxes to the continental scale by incorporating GEDI-derived canopy structural complexity metrics. *Remote Sens. Environ.* **329**, 114930 (2025).
131. Rannik, U. et al. in *Eddy Covariance: A Practical Guide to Measurement and Data* Analysis (eds Aubinet, M., Vesala, T. & Papale, D.) 8, 211–261 (Springer, 2012).
132. Gockede, M. et al. Quality control of CarboEurope flux data — part 1: coupling footprint analyses with flux data quality assessment to evaluate sites in forest ecosystems. *Biogeosciences* **5**, 433–450 (2008).
133. Kim, J. et al. Upscaling fluxes from tower to landscape: overlaying flux footprints on high-resolution (IKONOS) images of vegetation cover. *Agric. For. Meteorol.* **136**, 132–146 (2006).
134. Fu, D. et al. Estimating landscape net ecosystem exchange at high spatial–temporal resolution based on Landsat data, an improved upscaling model framework, and eddy covariance flux measurements. *Remote Sens. Environ.* **141**, 90–104 (2014).
135. Zhuravlev, R., Dara, A., dos Santos, A. L., Demidov, O. & Burba, G. Globally scalable approach to estimate net ecosystem exchange based on remote sensing, meteorological data, and direct measurements of eddy covariance sites. *Remote Sens.* **14**, 5529 (2022).
136. Papale, D. et al. Effect of spatial sampling from European flux towers for estimating carbon and water fluxes with artificial neural networks. *J. Geophys. Res.* **120**, 1941–1957 (2015).
137. Tramontana, G., Ichii, K., Camps-Valls, G., Tomelleri, E. & Papale, D. Uncertainty analysis of gross primary production upscaling using random forests, remote sensing and eddy covariance data. *Remote Sens. Environ.* **168**, 360–373 (2015).
138. Zeng, J. Y. et al. Global terrestrial carbon fluxes of 1999–2019 estimated by upscaling eddy covariance data with a random forest. *Sci. Data* **7**, G00J07 (2020).
139. Ueyama, M. et al. Upscaling terrestrial carbon dioxide fluxes in Alaska with satellite remote sensing and support vector regression. *J. Geophys. Res.* **118**, 1266–1281 (2013).
140. Ichii, K. et al. New data-driven estimation of terrestrial CO_2 fluxes in Asia using a standardized database of eddy covariance measurements, remote sensing data, and support vector regression. *J. Geophys. Res.* **122**, 767–795 (2017).
141. Yang, F. H. et al. Prediction of continental-scale evapotranspiration by combining MODIS and AmeriFlux data through support vector machine. *IEEE Trans. Geosci. Remote Sens.* **44**, 3452–3461 (2006).
142. Zhu, S. Y., Quaife, T. & Hill, T. Uniform upscaling techniques for eddy covariance FLUXes (UFLUX). *Int. J. Remote Sens.* **45**, 1450–1476 (2024).
143. Shangguan, W. et al. A 1 km global carbon flux dataset using in situ measurements and deep learning. *Forests* **14**, 913 (2023).
144. Fan, B. et al. Estimating carbon fluxes over North America using a physics-constrained deep learning model. *ISPRS J. Photogramm. Remote Sens.* **227**, 551–569 (2025).
145. Tramontana, G. et al. Predicting carbon dioxide and energy fluxes across global FLUXNET sites with regression algorithms. *Biogeosciences* **13**, 4291–4313 (2016).
146. Huang, C. C. et al. Exploring the potential of long short-term memory networks for predicting net CO_2 exchange across various ecosystems with multi-source data. *J. Geophys. Res.* **129**, e2023JD040418 (2024).
147. Xiao, J. F., Davis, K. J., Urban, N. M., Keller, K. & Saliendra, N. Z. Upscaling carbon fluxes from towers to the regional scale: Influence of parameter variability and land cover representation on regional flux estimates. *J. Geophys. Res.* **116**, G00J06 (2011).
148. Xiao, J. F., Davis, K. J., Urban, N. M. & Keller, K. Uncertainty in model parameters and regional carbon fluxes: a model–data fusion approach. *Agric. For. Meteorol.* **189**, 175–186 (2014).
149. Zhang, Y. Q. et al. Coupled estimation of 500 m and 8-day resolution global evapotranspiration and gross primary production in 2002-2017. *Remote Sens. Environ.* **222**, 165–182 (2019).
150. Chen, X., Su, Z., Ma, Y. & Middleton, E. M. Optimization of a remote sensing energy balance method over different canopy applied at global scale. *Agric. For. Meteorol.* **279**, 107633 (2019).
151. Virkkala, A. M. et al. Statistical upscaling of ecosystem CO_2 fluxes across the terrestrial tundra and boreal domain: regional patterns and uncertainties. *Glob. Change Biol.* **27**, 4040–4059 (2021).
152. Wang, Y., Tian, D., Xiao, J., Li, X. & Niu, S. Increasing drought sensitivity of plant photosynthetic phenology and physiology. *Ecol. Indic.* **166**, 112469 (2024).
153. Kondo, M., Ichii, K., Takagi, H. & Sasakawa, M. Comparison of the data-driven top-down and bottom-up global terrestrial CO_2 exchanges: GOSAT CO_2 inversion and empirical eddy flux upscaling. *J. Geophys. Res.* **120**, 1226–1245 (2015).
154. Flach, M. et al. Vegetation modulates the impact of climate extremes on gross primary production. *Biogeosciences* **18**, 39–53 (2021).
155. Beer, C. et al. Terrestrial gross carbon dioxide uptake: global distribution and covariation with climate. *Science* **329**, 834–838 (2010).
156. Badgley, G., Anderegg, L. D. L., Berry, J. A. & Field, C. B. Terrestrial gross primary production: using NIR_v to scale from site to globe. *Glob. Change Biol.* **25**, 3731–3740 (2019).
157. Zheng, Y. et al. Improved estimate of global gross primary production for reproducing its long-term variation, 1982–2017. *Earth Syst. Sci. Data* **12**, 2725–2746 (2020).
158. Xiao, J. F. et al. Assessing net ecosystem carbon exchange of US terrestrial ecosystems by integrating eddy covariance flux measurements and satellite observations. *Agric. For. Meteorol.* **151**, 60–69 (2011).
159. Yu, G., Chen, Z., Piao, S. & Zhu, X. High carbon dioxide uptake by subtropical forest ecosystems in the East Asian monsoon region. *Proc. Natl Acad. Sci. USA* **111**, 4910–4915 (2014).
160. Burton, C. A., Renzullo, L. J., Rifai, S. W. & Van Dijk, A. Empirical upscaling of OzFlux eddy covariance for high-resolution monitoring of terrestrial carbon uptake in Australia. *Biogeosciences* **20**, 4109–4134 (2023).
161. Pulliainen, J. et al. Increase in gross primary production of boreal forests balanced out by increase in ecosystem respiration. *Remote Sens. Environ.* **313**, 114376 (2024).
162. Watts, J. D. et al. Carbon uptake in Eurasian boreal forests dominates the high-latitude net ecosystem carbon budget. *Glob. Change Biol.* **29**, 1870–1889 (2023).
163. Xiao, J. F., Liu, S. G. & Stoy, P. C. Preface: impacts of extreme climate events and disturbances on carbon dynamics. *Biogeosciences* **13**, 3665–3675 (2016).
164. Zscheischler, J. et al. Carbon cycle extremes during the 21st century in CMIP 5 models: future evolution and attribution to climatic drivers. *Geophys. Res. Lett.* **41**, 8853–8861 (2014).
165. Ahlstrom, A. et al. The dominant role of semi-arid ecosystems in the trend and variability of the land CO_2 sink. *Science* **348**, 895–899 (2015).
166. Li, X. et al. New-generation geostationary satellite reveals widespread midday depression in dryland photosynthesis during 2020 western US heatwave. *Sci. Adv.* **9**, eadi0775 (2023).

167. Liang, W. et al. Grassland gross carbon dioxide uptake based on an improved model tree ensemble approach considering human interventions: global estimation and covariation with climate. *Glob. Change Biol.* **23**, 2720–2742 (2017).
168. Gampe, D. et al. Increasing impact of warm droughts on northern ecosystem productivity over recent decades. *Nat. Clim. Change* **11**, 772–779 (2021).
169. Duffy, K. et al. How close are we to the temperature tipping point of the terrestrial biosphere? *Sci. Adv.* **7**, eaay1052 (2021).
170. Tang, R. et al. Spatial-temporal patterns of land surface evapotranspiration from global products. *Remote Sens. Environ.* **304**, 114066 (2024).
171. Burnett, M. W., Quetin, G. R. & Konings, A. G. Data-driven estimates of evapotranspiration and its controls in the Congo Basin. *Hydrol. Earth Syst. Sci.* **24**, 4189–4211 (2020).
172. Li, W. et al. Contrasting drought propagation into the terrestrial water cycle between dry and wet regions. *Earths Future* **11**, e2022EF003441 (2023).
173. Fang, B., Lei, H., Zhang, Y., Quan, Q. & Yang, D. Spatio-temporal patterns of evapotranspiration based on upscaling eddy covariance measurements in the dryland of the North China Plain. *Agric. For. Meteorol.* **281**, 107844 (2020).
174. Buermann, W., Bikash, P. R., Jung, M., Burn, D. H. & Reichstein, M. Earlier springs decrease peak summer productivity in North American boreal forests. *Environ. Res. Lett.* **8**, 024027 (2013).
175. Nelson, J. A. et al. X-BASE: the first terrestrial carbon and water flux products from an extended data-driven scaling framework, FLUXCOM-X. *Biogeosciences* **21**, 5079–5115 (2024).
176. Martens, B. et al. GLEAM v3: satellite-based land evaporation and root-zone soil moisture. *Geosci. Model Dev.* **10**, 1903–1925 (2017).
177. Jung, M. et al. Recent decline in the global land evapotranspiration trend due to limited moisture supply. *Nature* **467**, 951–954 (2010).
178. Miralles, D. G. et al. El Niño–La Niña cycle and recent trends in continental evaporation. *Nat. Clim. Change* **4**, 122–126 (2014).
179. Cai, Y. H. et al. Reconciling global terrestrial evapotranspiration estimates from multi-product intercomparison and evaluation. *Water Resour. Res.* **60**, e2024WR037608 (2024).
180. Pan, S. F. et al. Evaluation of global terrestrial evapotranspiration using state-of-the-art approaches in remote sensing, machine learning and land surface modeling. *Hydrol. Earth Syst. Sci.* **24**, 1485–1509 (2020).
181. Wang, R. et al. Recent increase in the observation-derived land evapotranspiration due to global warming. *Environ. Res. Lett.* **17**, 024020 (2022).
182. Ma, N., Szilagyi, J. & Zhang, Y. Calibration-free complementary relationship estimates terrestrial evapotranspiration globally. *Water Resour. Res.* **57**, e2021WR029691 (2021).
183. Curtis, P. S. A meta-analysis of leaf gas exchange and nitrogen in trees grown under elevated carbon dioxide. *Plant Cell Environ.* **19**, 127–137 (1996).
184. Zhang, X. Z. et al. Greening-induced increase in evapotranspiration over Eurasia offset by CO_2-induced vegetational stomatal closure. *Environ. Res. Lett.* **16**, 124008 (2021).
185. Lu, X. L. & Zhuang, Q. L. Evaluating evapotranspiration and water-use efficiency of terrestrial ecosystems in the conterminous United States using MODIS and AmeriFlux data. *Remote Sens. Environ.* **114**, 1924–1939 (2010).
186. Yang, Y. T. et al. Contrasting responses of water use efficiency to drought across global terrestrial ecosystems. *Sci. Rep.* **6**, 23284 (2016).
187. Knauer, J. et al. The response of ecosystem water-use efficiency to rising atmospheric CO_2 concentrations: sensitivity and large-scale biogeochemical implications. *N. Phytol.* **213**, 1654–1666 (2017).
188. Guerrieri, R. et al. Disentangling the role of photosynthesis and stomatal conductance on rising forest water-use efficiency. *Proc. Natl Acad. Sci. USA* **116**, 16909–16914 (2019).
189. Richardson, A. D. et al. Statistical properties of random CO_2 flux measurement uncertainty inferred from model residuals. *Agric. For. Meteorol.* **148**, 38–50 (2008).
190. Lasslop, G., Reichstein, M., Kattge, J. & Papale, D. Influences of observation errors in eddy flux data on inverse model parameter estimation. *Biogeosciences* **5**, 1311–1324 (2008).
191. Ma, N., Zhang, Y. & Szilagyi, J. Water-balance-based evapotranspiration for 56 large river basins: a benchmarking dataset for global terrestrial evapotranspiration modeling. *J. Hydrol.* **630**, 130607 (2024).
192. Munger, J. W., Loescher, H. W. & Luo, H. in *Eddy Covariance: A Practical Guide to Measurement and Data Analysis* (eds Aubinet, M., Vesala, T. & Papale, D.) 21–58 (Springer, 2012).
193. Vitale, D., Bilancia, M. & Papale, D. Modelling random uncertainty of eddy covariance flux measurements. *Stoch. Environ. Res. Risk Assess.* **33**, 725–746 (2019).
194. Mauder, M. et al. A strategy for quality and uncertainty assessment of long-term eddy-covariance measurements. *Agric. For. Meteorol.* **169**, 122–135 (2013).
195. Richardson, A. D. et al. in *Eddy Covariance: A Practical Guide to Measurement and Data Analysis* (eds Aubinet, M., Vesala, T. & Papale, D.) 173–210 (Springer, 2012).
196. Alton, P. B. Representativeness of global climate and vegetation by carbon-monitoring networks; implications for estimates of gross and net primary productivity at biome and global levels. *Agric. For. Meteorol.* **290**, 108017 (2020).
197. Gamon, J. A., Serrano, L. & Surfus, J. S. The photochemical reflectance index: an optical indicator of photosynthetic radiation use efficiency across species, functional types, and nutrient levels. *Oecologia* **112**, 492–501 (1997).
198. Huete, A. et al. Overview of the radiometric and biophysical performance of the MODIS vegetation indices. *Remote Sens. Environ.* **83**, 195–213 (2002).
199. Badgley, G., Field, C. B. & Berry, J. A. Canopy near-infrared reflectance and terrestrial photosynthesis. *Sci. Adv.* **3**, e1602244 (2017).
200. Huang, X. J., Xiao, J. F. & Ma, M. G. Evaluating the performance of satellite-derived vegetation indices for estimating gross primary productivity using fluxnet observations across the globe. *Remote Sens.* **11**, 1823 (2019).
201. Rahman, A. F., Sims, D. A., Cordova, V. D. & El-Masri, B. Z. Potential of MODIS EVI and surface temperature for directly estimating per-pixel ecosystem C fluxes. *Geophys. Res. Lett.* **32**, L19404 (2005).
202. Frankenberg, C. et al. New global observations of the terrestrial carbon cycle from GOSAT: patterns of plant fluorescence with gross primary productivity. *Geophys. Res. Lett.* **38**, L17706 (2011).
203. Sun, Y. et al. OCO-2 advances photosynthesis observation from space via solar-induced chlorophyll fluorescence. *Science* **358**, eaam5747 (2017).
204. Li, X. et al. Solar-induced chlorophyll fluorescence is strongly correlated with terrestrial photosynthesis for a wide variety of biomes: first global analysis based on OCO-2 and flux tower observations. *Glob. Change Biol.* **24**, 3990–4008 (2018).
205. Li, X. & Xiao, J. F. TROPOMI observations allow for robust exploration of the relationship between solar-induced chlorophyll fluorescence and terrestrial gross primary production. *Remote Sens. Environ.* **268**, 112748 (2022).
206. Verma, M. et al. Effect of environmental conditions on the relationship between solar-induced fluorescence and gross primary productivity at an OzFlux grassland site. *J. Geophys. Res.* **122**, 716–733 (2017).
207. Zhang, Z. et al. Large diurnal compensatory effects mitigate the response of Amazonian forests to atmospheric warming and drying. *Sci. Adv.* **9**, eabq497 (2023).
208. Running, S. W. et al. A continuous satellite-derived measure of global terrestrial primary production. *Bioscience* **54**, 547–560 (2004).
209. Heinsch, F. A. et al. Evaluation of remote sensing based terrestrial productivity from MODIS using regional tower eddy flux network observations. *IEEE Trans. Geosci. Remote Sens.* **44**, 1908–1925 (2006).
210. Mu, Q., Heinsch, F. A., Zhao, M. & Running, S. W. Development of a global evapotranspiration algorithm based on MODIS and global meteorology data. *Remote Sens. Environ.* **111**, 519–536 (2007).
211. Cleugh, H. A., Leuning, R., Mu, Q. Z. & Running, S. W. Regional evaporation estimates from flux tower and MODIS satellite data. *Remote Sens. Environ.* **106**, 285–304 (2007).
212. Yuan, W. P. et al. Deriving a light use efficiency model from eddy covariance flux data for predicting daily gross primary production across biomes. *Agric. For. Meteorol.* **143**, 189–207 (2007).
213. Xiao, X. M. et al. Satellite-based modeling of gross primary production in an evergreen needleleaf forest. *Remote Sens. Environ.* **89**, 519–534 (2004).
214. Sasai, T., Ichii, K., Yamaguchi, Y. & Nemani, R. Simulating terrestrial carbon fluxes using the new biosphere model "biosphere model integrating eco-physiological and mechanistic approaches using satellite data" (BEAMS). *J. Geophys. Res.* **110**, G02014 (2005).
215. Mahadevan, P. et al. A satellite-based biosphere parameterization for net ecosystem CO_2 exchange: vegetation photosynthesis and respiration model (VPRM). *Glob. Biogeochem. Cycle* **22**, GB2005 (2008).
216. Volk, J. M. et al. Assessing the accuracy of OpenET satellite-based evapotranspiration data to support water resource and land management applications. *Nat. Water* **2**, 193–205 (2024).
217. Fisher, J. B. et al. ECOSTRESS: NASA's next generation mission to measure evapotranspiration from the international space station. *Water Resour. Res.* **56**, e2019WR026058 (2020).
218. Li, X., Xiao, J., Fisher, J. B. & Baldocchi, D. D. ECOSTRESS estimates gross primary production with fine spatial resolution for different times of day from the International Space Station. *Remote Sens. Environ.* **258**, 112360 (2021).
219. Ryu, Y., Jiang, C., Kobayashi, H. & Detto, M. MODIS-derived global land products of shortwave radiation and diffuse and total photosynthetically active radiation at 5 km resolution from 2000. *Remote Sens. Environ.* **204**, 812–825 (2018).
220. Zhang, X. T., Liang, S. L., Zhou, G. Q., Wu, H. R. & Zhao, X. Generating Global LAnd Surface Satellite incident shortwave radiation and photosynthetically active radiation products from multiple satellite data. *Remote Sens. Environ.* **152**, 318–332 (2014).
221. Liang, S. L. et al. Estimation of incident photosynthetically active radiation from moderate resolution imaging spectrometer data. *J. Geophys. Res.* **111**, D15208 (2006).
222. Yamamoto, Y., Ichii, K., Ryu, Y., Kang, M. & Murayama, S. Uncertainty quantification in land surface temperature retrieved from Himawari-8/AHI data by operational algorithms. *ISPRS J. Photogramm. Remote Sens.* **191**, 171–187 (2022).
223. Wu, H. R., Zhang, X. T., Liang, S. L., Yang, H. & Zhou, G. Q. Estimation of clear-sky land surface longwave radiation from MODIS data products by merging multiple models. *J. Geophys. Res.* **117**, D22107 (2012).
224. He, L., Qin, Q., Liu, M. & Dong, H. Validation of GLASS albedo products using ground measurements and landsat TM data. In *2012 IEEE International Geoscience and Remote Sensing Symposium* 1116–1119 (IEEE, 2012).
225. Cescatti, A. et al. Intercomparison of MODIS albedo retrievals and in situ measurements across the global FLUXNET network. *Remote Sens. Environ.* **121**, 323–334 (2012).
226. Gonsamo, A., Chen, J. M., Price, D. T., Kurz, W. A. & Wu, C. Y. Land surface phenology from optical satellite measurement and CO_2 eddy covariance technique. *J. Geophys. Res.* **117**, G03032 (2012).
227. Zhang, J. R. et al. Solar-induced chlorophyll fluorescence captures photosynthetic phenology better than traditional vegetation indices. *ISPRS J. Photogramm. Remote Sens.* **203**, 183–198 (2023).
228. Richardson, A. D., Hufkens, K., Milliman, T. & Frolking, S. Intercomparison of phenological transition dates derived from the PhenoCam Dataset V1.0 and MODIS satellite remote sensing. *Sci. Rep.* **8**, 5679 (2018).

229. Zhang, L. et al. Evaluation of the Community Land Model simulated carbon and water fluxes against observations over ChinaFLUX sites. *Agric. For. Meteorol.* **226**, 174–185 (2016).
230. Wang, W. et al. Quantifying the effects of harvesting on carbon fluxes and stocks in northern temperate forests. *Biogeosciences* **11**, 6667–6682 (2014).
231. Deng, J. et al. Improving a biogeochemical model to simulate surface energy, greenhouse gas fluxes, and radiative forcing for different land use types in northeastern United States. *Glob. Biogeochem. Cycle* **34**, e2019GB006520 (2020).
232. Schaefer, K. et al. A model–data comparison of gross primary productivity: results from the North American carbon program site synthesis. *J. Geophys. Res.* **117**, G03010 (2012).
233. Ichii, K. et al. Site-level model–data synthesis of terrestrial carbon fluxes in the CarboEastAsia eddy-covariance observation network: toward future modeling efforts. *J. For. Res.* **18**, 13–20 (2013).
234. MacBean, N. et al. Dynamic global vegetation models underestimate net CO_2 flux mean and inter-annual variability in dryland ecosystems. *Environ. Res. Lett.* **16**, 094023 (2021).
235. Huntzinger, D. N. et al. North American Carbon Program (NACP) regional interim synthesis: terrestrial biospheric model intercomparison. *Ecol. Model.* **232**, 144–157 (2012).
236. Anav, A. et al. Evaluating the land and ocean components of the global carbon cycle in the CMIP5 Earth system models. *J. Clim.* **26**, 6801–6843 (2013).
237. Li, J. D. et al. Evaluation of CMIP6 global climate models for simulating land surface energy and water fluxes during 1979-2014. *J. Adv. Model. Earth Syst.* **13**, e2021MS002515 (2021).
238. Deng, F. et al. The use of forest stand age information in an atmospheric CO_2 inversion applied to North America. *Biogeosciences* **10**, 5335–5348 (2013).
239. Upton, S. et al. Constraining biospheric carbon dioxide fluxes by combined top-down and bottom-up approaches. *Atmos. Chem. Phys.* **24**, 2555–2582 (2024).
240. Madani, N., Kimball, J. S. & Running, S. W. Improving global gross primary productivity estimates by computing optimum light use efficiencies using flux tower data. *J. Geophys. Res.* **122**, 2939–2951 (2017).
241. Williams, M. et al. Improving land surface models with FLUXNET data. *Biogeosciences* **6**, 1341–1359 (2009).
242. Huang, X., Xiao, J., Ma, M. & Wang, X. Improving the global MODIS GPP model by optimizing parameters with FLUXNET data. *Agric. For. Meteorol.* **300**, 108314 (2021).
243. Braswell, B. H., Sacks, W. J., Linder, E. & Schimel, D. S. Estimating diurnal to annual ecosystem parameters by synthesis of a carbon flux model with eddy covariance net ecosystem exchange observations. *Glob. Change Biol.* **11**, 335–355 (2005).
244. Williams, M., Schwarz, P. A., Law, B. E., Irvine, J. & Kurpius, M. R. An improved analysis of forest carbon dynamics using data assimilation. *Glob. Change Biol.* **11**, 89–105 (2005).
245. Wang, Y. P., Baldocchi, D., Leuning, R., Falge, E. & Vesala, T. Estimating parameters in a land-surface model by applying nonlinear inversion to eddy covariance flux measurements from eight FLUXNET sites. *Glob. Change Biol.* **13**, 652–670 (2007).
246. Stockli, R. et al. Use of FLUXNET in the Community Land Model development. *J. Geophys. Res.* **113**, G01025 (2008).
247. Ichii, K. et al. Refinement of rooting depths using satellite-based evapotranspiration seasonality for ecosystem modeling in California. *Agric. For. Meteorol.* **149**, 1907–1918 (2009).
248. Bonan, G. B. et al. Improving canopy processes in the Community Land Model version 4 (CLM4) using global flux fields empirically inferred from FLUXNET data. *J. Geophys. Res.* **116**, G02014 (2011).
249. Papale, D. Ideas and perspectives: enhancing the impact of the FLUXNET network of eddy covariance sites. *Biogeosciences* **17**, 5587–5598 (2020).
250. Liang, M. C. et al. New constraints of terrestrial and oceanic global gross primary productions from the triple oxygen isotopic composition of atmospheric CO_2 and O_2. *Sci. Rep.* **13**, 2162 (2023).
251. Baldocchi, D. D. Assessing the eddy covariance technique for evaluating carbon dioxide exchange rates of ecosystems: past, present and future. *Glob. Change Biol.* **9**, 479–492 (2003).
252. Novick, K. A. et al. Informing nature-based climate solutions for the United States with the best-available science. *Glob. Change Biol.* **28**, 3778–3794 (2022).
253. Hemes, K. S., Runkle, B. R. K., Novick, K. A., Baldocchi, D. D. & Field, C. B. An ecosystem-scale flux measurement strategy to assess natural climate solutions. *Environ. Sci. Technol.* **55**, 3494–3504 (2021).
254. Rebmann, C. et al. ICOS eddy covariance flux-station site setup: a review. *Int. Agrophysics* **32**, 471–494 (2018).
255. DE-HoH_team. *DE-HoH ICOS Ecosystem Station* (ICOS, accessed 29 March 2025); https://meta.icos-cp.eu/resources/stations/ES_DE-HoH.
256. FI-Sii_team. *FI-Sii ICOS Ecosystem Station* (ICOS, accessed 29 March 2025); https://meta.icos-cp.eu/resources/stations/ES_FI-Sii.
257. Schmid, H. P. & Lloyd, C. R. Spatial representativeness and the location bias of flux footprints over inhomogeneous areas. *Agric. For. Meteorol.* **93**, 195–209 (1999).
258. Kljun, N., Calanca, P., Rotach, M. W. & Schmid, H. P. A simple two-dimensional parameterisation for flux footprint prediction (FFP). *Geosci. Model. Dev.* **8**, 3695–3713 (2015).
259. Kroon, P. S. et al. Uncertainties in eddy covariance flux measurements assessed from CH_4 and N_2O observations. *Agric. For. Meteorol.* **150**, 806–816 (2010).
260. About the FLUXNET network. *FLUXNET* (accessed 8 October 2025); https://fluxnet.org/about/.

Acknowledgements
J.X. thanks the National Science Foundation (Macrosystem Biology and NEON-Enabled Science program: DEB-2017870), Google and the Iola Hubbard Climate Change Endowment for support. D.B. thanks the US DOE AmeriFlux Management Project and its support of core sites for support. F.L. thanks the National Natural Science Foundation of China (grant no. 42471426) for support. K.I. thanks JSPS Core-to-Core Program (grant no. JPJSCCA20220008), JSPS Kakenhi (grant no. JP22H05004) and Environment Research and Technology Development Fund (grant no. JPMEERF24S12207) of the Environmental Restoration and Conservation Agency provided by Ministry of the Environment of Japan for support. D.P. thanks the EU Next Generation EU Mission 4 'Education and Research', project IR0000032; ITINERIS, Italian Integrated Environmental Research Infrastructures System CUP B53C22002150006 for support. K.I. thanks M. Hase and A. Kosugo for graphic support. D.P. thanks the ICOS Ecosystem Thematic Centre and the OEMC HEurope project (GA 101059548) for support.

Author contributions
J.X. conceptualized and led the study, with substantial contributions to the outline and design from D.B., K.I., F.L. and D.P. All authors substantially contributed to data research and analysis, discussion, drafting and revision of the manuscript.

Competing interests
The authors declare no competing interests.

Additional information
Supplementary information The online version contains supplementary material available at https://doi.org/10.1038/s43017-025-00743-1.

Peer review information *Nature Reviews Earth & Environment* thanks Ning Ma and the other, anonymous, reviewer(s) for their contribution to the peer review of this work.

Related links
La Thuile 2007: https://fluxnet.org/data/la-thuile-dataset/
Marconi 2000: https://doi.org/10.3334/ornldaac/811